University of Genoa

STUDY COURSE IN BIOENGINEERING

CURRICULUM NEUROENGINEERING AND BIO-ICT

Degree thesis for the achievement of the title of

Master's Degree in Bioengineering

Towards brain-like models in vitro: from 2D to 3D cultures

Lorenzo Corsello

date 06/14/23

Supervisor: Prof. Laura Pastorino

Supervisor: Prof. Michela Chiappalone

Co-Supervisor : Dr. Donatella Di Lisa

Index

Introduction

Nervous system disorders are estimated to affect more than one billion people worldwide (Pai, 2009). Typical examples of nerve disorders include acute traumatic injuries (e.g., head trauma, spinal cord injury), neurodegenerative diseases (e.g., Parkinson's disease, Alzheimer's disease, Huntington's disease), or neurodevelopmental disorders such as microcephaly and autism.

In almost all cases there is no effective treatment. The lack of adequate experimental models that summarize the complex cell-cell and cell-environment interactions *in vivo* hinders the development of new therapeutic interventions.

The challenge facing biomedical engineering is the development of advanced models of the central nervous system able to improve the understanding of neurophysiology, the pathogenesis of neurodegenerative diseases and at the same time explore new possible therapies.

Current studies of brain physiology have largely been conducted using *in vivo* animal models or primary rodent cell cultures grown on a two-dimensional (2D) substrate. While these models have provided insight into the complex interactions between brain cell types, they have some specific key drawbacks and differences with the human model.

At the genomic level, for example, despite the large number of orthologous genes between humans and mice, there are genes or gene functions associated with various diseases specific to humans. At the cellular level, the differences between human and mouse brains are found, for example, in glial cell populations, as characteristics such as the ratio of astrocytes to neurons and the complexity of astrocytes are both markedly higher in the human brain.

The use of traditional *in vitro models* of animal origin has provided a wealth of information on neural cells; for example, spontaneous network formation, cell attachment sites for adhesion and migration, axon guidance mechanisms, molecules in synaptic targeting and the resting membrane potential of different cell types.

Furthermore, to better mimic the complex connectivity present in the human brain, much effort has been devoted to constructing *in vitro* controllable neuronal structures with a three-dimensional (3D) architecture.

The main objective of this thesis is the development and characterization of *in vitro* 2D and 3D networks formed by neurons, differentiated from human induced pluripotent stem cells (human-induced pluripotent stem cells, ie h-iPSC), in co-culture with rat cortical astrocytes.

The 3D culture is ensured by the use of a thermosensitive biopolymer hydrogel, in which the cells are encapsulated.

Spontaneous activity of 2D and 3D networks was captured at different points in development by microelectrode array (MEA) devices. The possibility of using an acquisition system based on probes, typically used for *in vivo* recordings, capable of penetrating 3D tissue, was evaluated and explored.

The main activities of the thesis include:

- *In vitro* experiments: Experiments with 2D and 3D *in vitro* cultures of neurons and astrocytes with acquisitions of spontaneous electrophysiological activity by means of microelectrode arrays.
- Morphological image analysis: The immunofluorescence technique was used to mark and visualize the different components of the cell cultures and verify the formation of the networks.
- Data Processing: Neuronal data were processed using algorithms in MATLAB.
- Comparative analysis and data interpretation: Data from 2D and 3D cultures were compared and a profile of functional development was provided for each experimental group.

The thesis is organized in the following chapters:

- Chapter 1. Bases of Neurophysiology and Experimental Models: In which some basics of neurophysiology are given and the state of the art of experimental models is presented.
- Chapter 2. Tools for Data Analysis: In which the tools and algorithms used for data analysis are presented.
- Chapter 3. Materials and Experimental Methods: In which the materials and methods used for the preparation and characterization of cultures are presented.
- Chapter 4. Results: In which the experimental results obtained are presented and discussed, both as regards the electrophysiological and morphological analysis.

The knowledge gained during this project will help to understand the electrophysiological phenotypes of 2D and 3D cultures and will allow us to take a step towards the development of neural models to be exploited for patient-specific therapies.

Chapter 1

1. Bases of Neurophysiology and Experimental Models

1.1 Nervous system and blood brain barrier

The nervous system is one of the most important and complex systems in the human body. It is a network of specialized cells, tissues and organs that transmit electrical and chemical signals throughout the body. These signals allow the body to respond to internal and external stimuli, coordinate and control various functions, and maintain homeostasis.

The nervous system is divided into two main parts: the central nervous system (CNS) (Figure 1.1(a)) and the peripheral nervous system (PNS) (Figure 1.1(b)). The CNS, which is made up of the brain and spinal cord, is responsible for processing and interpreting information received from the sensory systems, and also controls the body's responses to stimuli. The PNS, on the other hand, is made up of nerves and ganglia and is responsible for carrying information from the CNS to the organs of the body and vice versa.

The brain, which is the most complex organ in the body, is the main control center for the nervous system. It receives, processes and interprets information received from the senses and then sends commands to the rest of the body through the spine (or spinal cord). The spinal cord, which is a long, delicate tube of nerve tissue that runs from the base of the brain down to the lower back, serves as a relay station for signals traveling to and from the brain.

The PNS is further divided into two subsystems: the somatic and autonomic nervous systems. The somatic nervous system controls voluntary body movements and sensations, such as limb movements and the sensation of touch. The autonomic nervous system, on the other hand, controls involuntary body functions, such as heart rate, digestion, and breathing.

The nervous system plays a crucial role in maintaining homeostasis, which is the balance of internal conditions in the body. It does this by continuously monitoring the internal and external environment of the body and making necessary changes. For example, the nervous system

regulates body temperature, blood pressure, and heart rate to ensure they stay within a normal range.

In general, the nervous system is an incredibly complex system, but for the purposes of this thesis it will suffice to focus on neurons, astrocytes and the extracellular matrix.

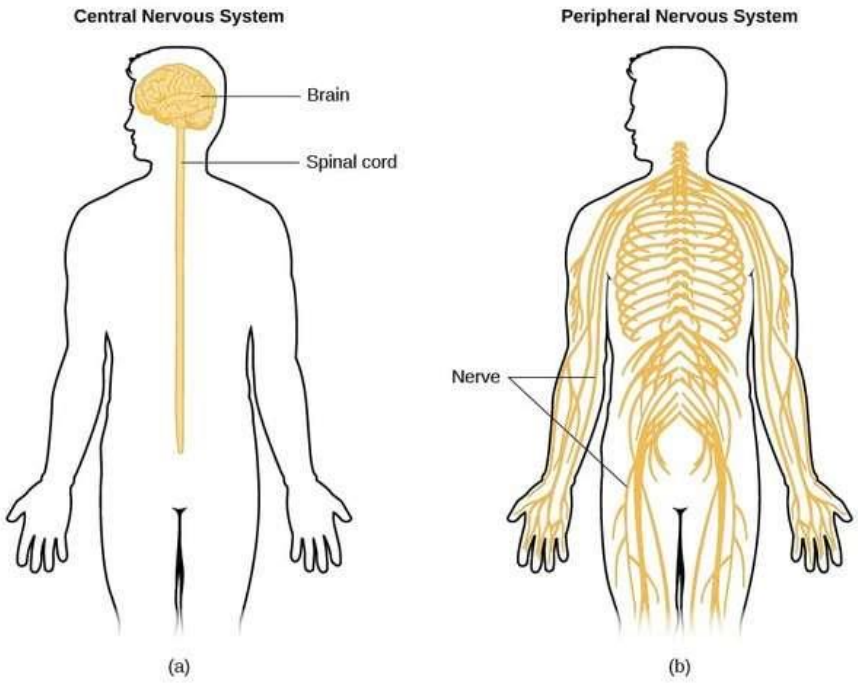

Figure 1.1 (a) Central Nervous System, (b) Peripheral Nervous System

1.1.1 Neurons

Neurons are the functional units of the nervous system, they are responsible for the generation and transmission of electrical impulses, known as action potentials.

Structure of Neurons

Neurons are composed of three main components (Figure 1.2): the cell body (soma), cytoplasmic extensions called dendrites, and a further extension called the axon. The cell body contains the nucleus and other cellular components essential for the functioning of the neuron. Dendrites branch off from the cell body and receive signals from other neurons or sensory cells. The axon is a single, long extension that carries out signals from the neuron to other neurons or to effector organs.(Bear et al., 2015)

Synapse

Synapses are the specialized junctions between the axon of one neuron, called the synaptic terminal, and the dendrite or soma of another neuron. Communication between neurons occurs through these synapses. There are two main types of synapses: electrical and chemical.

Electrical synapses allow for the direct passage of electrical signals between neurons across gap junctions. In contrast, chemical synapses involve the transmission of chemical signals called neurotransmitters.(Shepherd, 2004)

Neurotransmitters

Neurotransmitters are chemical molecules involved in signal transmission between neurons. They can be classified as excitatory or inhibitory neurotransmitters depending on the effects they have on the postsynaptic cell. Some examples of excitatory neurotransmitters include glutamate, acetylcholine, and adrenaline, while GABA and glycine are examples of inhibitory neurotransmitters.(Boyle, 2005)

Glutamate

Glutamate is the major excitatory neurotransmitter in the central nervous system. It plays a key role in learning, memory, and the transmission of sensory signals. Glutamate acts by binding to glutamate receptors on the postsynaptic membrane, such as NMDA (N-methyl-D-aspartate) receptors and AMPA (α-amino-3-hydroxy-5-methyl-4-isoxazole propionate) receptors, causing a depolarization of the target cell.(Mayer, 2005)

GABA

γ-Aminobutyric acid (GABA) is the major inhibitory neurotransmitter in the central nervous system. GABA acts by binding to GABA receptors on the postsynaptic membrane and induces hyperpolarization of the target cell, reducing the likelihood of generating an action potential. GABA plays a fundamental role in the control of muscle tone, sleep regulation and anxiety.(Petroff, 2002)

Synaptic plasticity

Synaptic plasticity refers to the ability of synapses to change their strength and efficiency over time. Synaptic plasticity underlies learning and memory processes in the brain. Short-term synaptic plasticity acts on a time scale from tens of milliseconds to a few minutes in contrast to long-term plasticity, which lasts from minutes to hours. An important mechanism of synaptic plasticity is long-term plasticity, classified into long-term potentiation (LTP) and long-term depression (LTD). LTP is a long-term increase in synaptic efficiency, while LTD is a long-

term decrease in synaptic efficiency. These processes depend on the modulation of neurotransmitters and the strengthening or weakening of synapses.(Malenka & Bear, 2004)

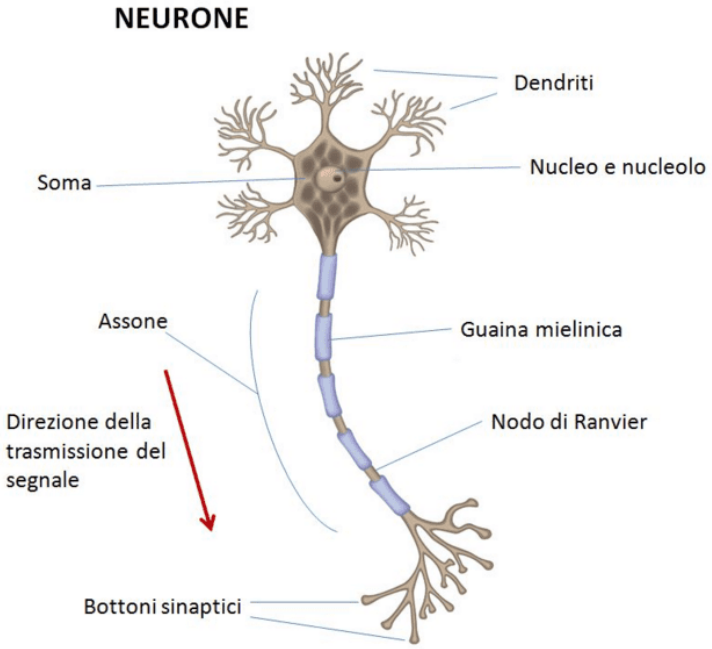

Figure 1.2 Schematic representation of a neuron

1.1.2 Astrocytes

The primary role of astrocytes (Figure 1.3) is to provide structural and functional support to neurons, to regulate extrasynaptic neurotransmitter levels, and to modulate specific steps in synapse formation and plasticity (Freeman, 2010).

Astrocytes and neurons are in a constant feedback loop through the release of neurotransmitters, such as GABA and glutamate, which modulate synaptic transmission and the electrochemical behavior of both cell types. The interconnected group of a pre- and post-synaptic neuron and astrocyte is referred to as a tripartite synapse (Araque et al., 1999). Neuronal firing activity induces the release of glutamate and γ-aminobutyric acid from pre-synaptic neurons (Mayorquin et al., 2018; Verkhratsky & Nedergaard, 2018). When glutamate binds to metabotropic glutamate receptors (mGluRs) on the astrocytic cell membrane, a cascade of chemical reactions results in the release of the second messenger inositol triphosphate (IP3), which in turn triggers the intracellular release of [Ca^{2+}] (Bazargani & Attwell, 2016). The increase in [Ca^{2+}], elicited by glutamate or GABA uptake, can result in the release of gliotransmitters that regulate synaptic transmission and synaptic plasticity of neurons (Araque et al., 1999).

Astrocytes are non-proliferative in the normal adult brain, however, upon injury, these cells can be activated. Astrocyte cells are activated under certain pathological conditions which can be identified by a high level of glial fibrillary acid protein (GFAP) expression (Gomi et al., 2010; Li et al., 2008).

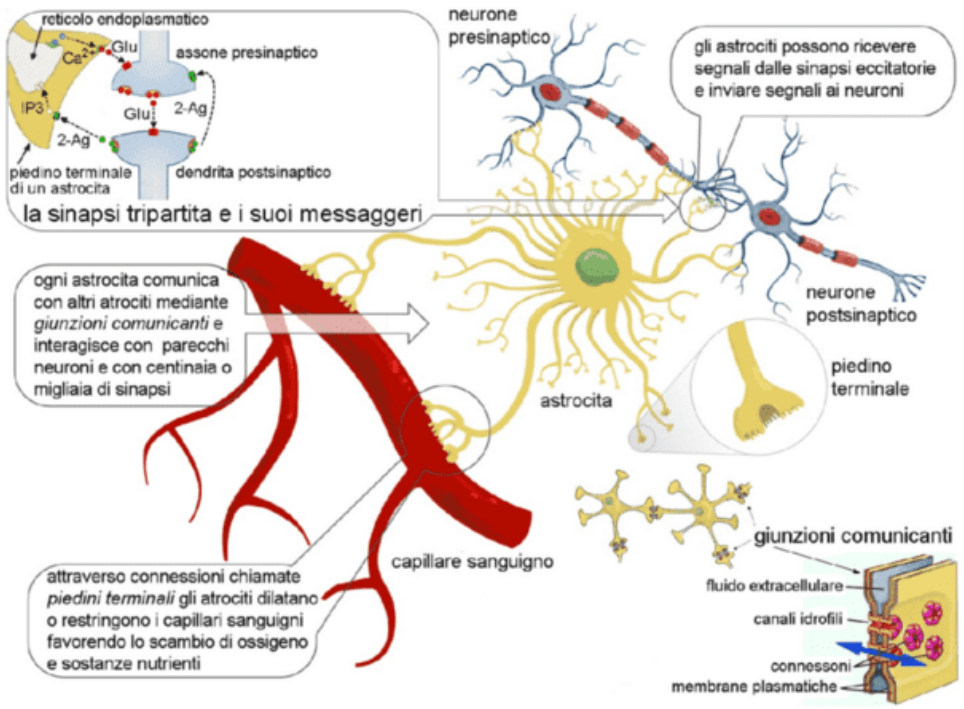

Figure 1.3 Schematic representation of an astrocyte and its main properties. (Nobili, Renato. (2015). The machine of the mind. II - The role of synchronization in the functioning of the brain.)

1.1.3 Extracellular matrix of the central nervous system

The central nervous system is mainly formed by cells and blood vessels and for the remaining part (15-25% of the volume) by the extracellular space which is made up of the extracellular matrix (ECM) for 20% (Nicholson & Syková, 1998).

The extracellular matrix of the central nervous system (Figure 1.4) influences cell proliferation, differentiation, migration and maturation during brain development.

The composition of the extracellular matrix in the nervous system is particular: Unlike the extracellular matrices of other tissues, the native extracellular matrix of the brain presents a complex microenvironment composed mainly of hyaluronic acid, proteoglycans, tenascins, linking proteins, laminins, fibronectins and collagens (Novak & Kaye, 2000).

In addition to serving as a structural support for cells, the extracellular matrix also provides extrinsic signals to regulate cellular behavior. In particular, the mechanical property of the

ECM is an essential parameter that must be considered when designing in vitro tissue surrogates, neuronal tissues possess very distinct biophysical properties, such as low elastic modulus, much lower than heart, cartilage and bone.

Numerous evidences (Engler et al., 2006; Georges & Janmey, 2005) have demonstrated that matrix stiffness elicits relevant effects on cellular morphologies and behaviors, in particular, it is probable that nerve stem cells differentiate into glial cells when incorporated into matrices with higher modulus (<1 kPa), while softer gels (100-500 Pa) tend to improve cell migration and differentiation into neurons.

Similarly, matrix porosity greatly influences cell migration and metabolic efficiency, for example, large pore size (more than 100 μm) and better interconnectivity improved nutrient exchange; proper pore size, similar to that of native tissues, leads to improved cell migration.

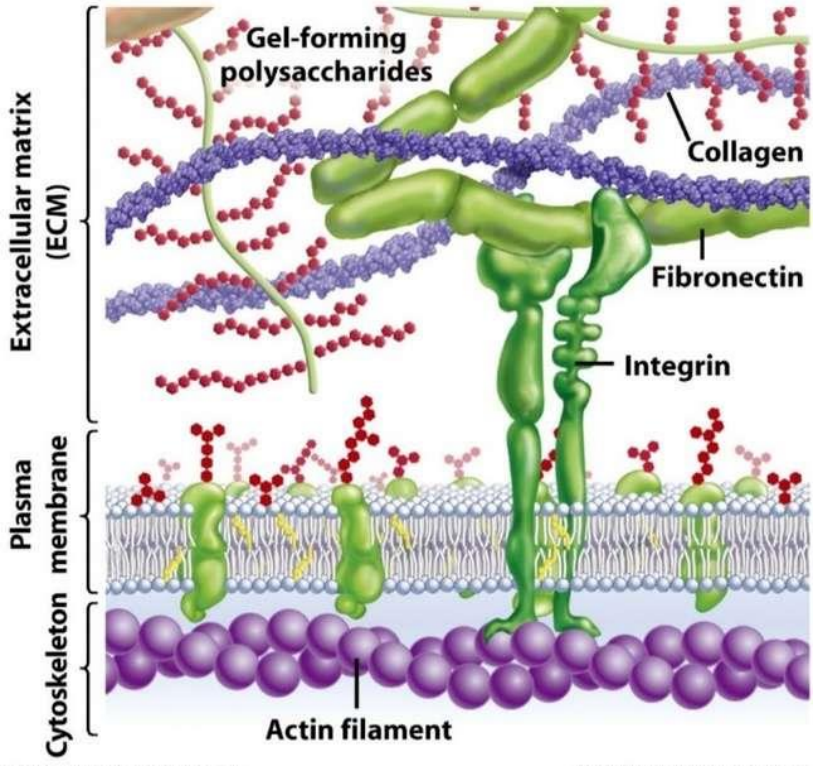

Figure 1.4 Schematic representation of the extracellular matrix

1.1.4 Spontaneous Electrophysiological Activity of the Central Nervous System

Spontaneous CNS activity can be divided into two main categories: background activity and synchronized spontaneous activity.

Background activity

The underlying activity is the spontaneous, continuous, and irregular activity of the CNS in the absence of external stimuli. This activity is characterized by low-frequency action potentials, typically between 1 and 10 Hz, that occur randomly in different regions of the brain. This activity is present in all regions of the CNS and can be recorded *in vivo* and *in vitro.* Background activity has been observed in all vertebrates from fish to mammals, including humans (Hughes et al., 2002).

Synchronized spontaneous activity

Synchronized spontaneous activity is spontaneous activity in which neurons of a particular brain region fire simultaneously in a synchronized manner. This type of activity is present in several brain regions and can be recorded both *in vivo* and *in vitro.* The synchronized spontaneous activity occurs at a higher frequency than the background activity and can be divided into three main categories: local field oscillations, slow waves and high frequency oscillations (Buzsáki, 2006) .

Local field oscillations

Local field potential (LFP) oscillations are low frequency oscillations (0.1-200 Hz) recorded by the recording electrode as a sum of the electrical events of surrounding neurons (Buzsáki, 2006). These oscillations occur in different regions of the brain and can be divided into different frequency bands, including delta (1-4Hz), theta (4-8Hz), alpha (8-12Hz), beta (12-30Hz). Hz) and range (30-100 Hz) (Buzsáki, 2006). Local field oscillations are associated with several physiological and behavioral states, including sleep, wakefulness, and cognition (Buzsáki, 2006).

Slow waves

Slow waves are low-frequency (0.5-4Hz) oscillations recorded in different regions of the brain, including the forebrain and hindbrain (Steriade et al., 1993). These waves are characterized by a period of hyperpolarization followed by a period of depolarization leading to the generation of action potentials. Slow waves are typically seen in different stages of sleep, particularly in slow deep sleep (NREM) (Mölle et al., 2002), but are also present during wakefulness and can be seen in anesthetized animals (Steriade et al., 1993). Slow waves have an important function in memory consolidation, as they have been shown to be essential for long-term memory formation (Diekelmann & Born, 2010).

Theta waves

Theta waves are low-frequency (4-8 Hz) oscillations that are present in several regions of the brain, including the hippocampus and medial prefrontal cortex. These waves are often associated with awake activity and are recorded during spatial navigation and episodic memory (Buzsáki, 2002). Additionally, theta waves have been observed during REM sleep and during the exploration of new environments by animals (Buzsáki, 2002).

Epileptiform activity

Epileptiform activity is a type of spontaneous activity that occurs when neurons in the brain fire synchronous and abnormal firing of action potentials. This activity can be observed in epilepsy patients and in animal models of epilepsy (Avoli et al., 2002). Epileptiform activity can be of several types, including spike-and-wave discharges that occur during generalized seizures, and paroxysmal discharges that occur in certain regions of the brain during focal seizures(Avoli et al., 2002)

Regulation of spontaneous activity

Spontaneous CNS activity is regulated by several mechanisms, including the balance between synaptic excitation and inhibition, synaptic plasticity, the activity of neuromodulators and circadian rhythms.

Balance between synaptic excitation and inhibition

Synaptic excitation and inhibition are the building blocks of spontaneous CNS activity. Excitation is mediated by the action of excitatory neurotransmitters such as glutamate on ionotropic receptors, while inhibition is mediated by the action of inhibitory neurotransmitters such as GABA and glycine on ionotropic receptors (Roth & Draguhn, 2012). The balance between synaptic excitation and inhibition is essential to regulate the spontaneous activity of the CNS and prevent the onset of pathologies such as epilepsy.

Synaptic plasticity

Synaptic plasticity is a fundamental mechanism for the regulation of spontaneous CNS activity, as it allows neuronal connections to adapt to changes in sensory input and experience. Plasticity is divided into two main classes: short-term synaptic plasticity, and long-term synaptic plasticity. Short-term synaptic plasticity acts on a time scale from tens of milliseconds to a few minutes in contrast to long-term plasticity, which lasts from minutes to hours.

Long-term synaptic plasticity can be classified into two types: long-term potentiation (LTP) and long-term depression (LTD) (Bear & Malenka, 1994).

LTP is a process of potentiation of synaptic strength that occurs after a repetition of high-frequency stimulation. This phenomenon was first described in 1973 by Bliss and Lomo (Bliss & Lømo, 1973) and was later identified in several brain regions, including the hippocampus (Bliss & Collingridge, 1993). LTP is mediated by several mechanisms, including the activation of NMDA (N-methyl-D-aspartate) receptors, which leads to the entry of calcium ions into postsynaptic cells and the activation of intracellular signal transduction (Bear & Malenka, 1994). LTP has been implicated in several cognitive processes, including learning and memory (Whitlock et al., 2006).

LTD, on the other hand, is a process of decreased synaptic strength that occurs after one repetition of low-frequency stimulation. LTD has also been described in different brain regions and may be mediated by several mechanisms, including the activation of metabotropic glutamate receptors (mGluR) and the consequent reduction of postsynaptic activity (Bear & Malenka, 1994). LTD has been implicated in several processes, including depression and the purging of unnecessary memories (Dudek & Bear, 1992).

Furthermore, synaptic plasticity is also modulated by epigenetic factors, such as histone acetylation and DNA methylation (Day & Sweatt, 2011). These mechanisms can influence the expression of genes involved in synaptic plasticity and regulate the effectiveness of synapses.

1.2 Models of nervous tissue *in vitro*

The study of neurons, through *in vitro* cultures, was conducted for the first time in 1907 thanks to the contribution of Ross Harrison (Harrison et al., 1907)who, through tissue culture, kept alive the tissue explants outside the animal by observing the nerve cell development. *In vitro* models can be divided into two-dimensional (2D) and three-dimensional (3D) cultures.

2D culture involves the adhesion and growth of cells on a glass monolayer (slides, microelectrode array devices) or, more commonly, polystyrene plastic (petri dishes, flasks) for tissue culture. The main disadvantage of this technique is that it fails to replicate the three-dimensional cell-ECM interactions that normally occur *in vivo*.

To overcome this limitation, 3D cultures were introduced in 1980, with the aim of better mimicking the *in vivo* cellular environment. This technique involves growing cells in a three-

dimensional scaffold/matrix or immersed in a suspended medium in the form of 3D aggregates/spheroids (Chaicharoenaudomrung et al., 2019).

A further step forward in the development of reliable models has been represented by the introduction of human-derived pluripotent stem cells (hPSC). These cells are capable of self-renewal and differentiate into all three germ layers: the endoderm, mesoderm and ectoderm. hPSCs are divided into human embryonic stem cells (hESCs) and human induced pluripotent stem cells (hIPSCs). The neural differentiation of hPSCs was first described in 2001 and since then, a large number of differentiation protocols have been published that direct the development of hPSCs towards neural cells (Carpenter et al., 2001; Reubinoff et al., 2001).

In order to study the nervous system, neuronal cultures require the use of components of the extracellular matrix, such as for example laminin, fibronectin, polyornithine, or other adhesion factors, such as natural polymers including chitosan, which has proved to be very effective for neuritic outgrowth *in vitro* (Di Lisa et al., 2022; Hagg et al., 1989; Hatten et al., 1982).

1.2.1 Scaffolding

The concept of "scaffolding" in relation to *in vitro* neuron cultures, refers to the use of a support structure to guide and shape the growth and organization of neural cells in a laboratory setting. This may include the use of extracellular matrix (ECM) components, such as laminin, hyaluronic acid and collagen, synthetic materials such as polyethylene glycol (PEG) and poly-L-lysine (PLL), natural materials such as chitosan and alginate, and semi-synthetic such as gelatin methacrylate (GELMA) or hyaluronic acid methacrylate (HAMA)

The scaffold provides the suitable environment for the cells to be able to effectively carry out their tasks such as adhesion, proliferation and differentiation.

To perform these various functions in tissue engineering, the scaffold must meet the following requirements:

• Biocompatibility,

• Biodegradability

• Non-toxic and non-immunogenic.

• Appropriate porosity and morphology for the transport of cells, gases, metabolites, nutrients and signal molecules both within the scaffold and between the scaffold and the surrounding environment.

In this context, chitosan-based hydrogel is considered as a good candidate for a broad spectrum of applications as it possesses unique biological properties including bioactivity, biocompatibility, biodegradability, non-toxicity, physiological inertness, antibacterial, hemostatic, fungistatic, and anticancer properties.

1.2.1.1 Hydrogels

Hydrogels (Figure 1.5) are three-dimensional polymeric networks, capable of absorbing and retaining large amounts of water (>90%) (Buwalda et al., 2014).

Commonly hydrogels are characterized by: (1) hydrogen bonds, (2) electrostatic interactions, (3) hydrophobic interactions, (4) water-mediated hydrogen bonds, (5) van der Waals interactions, (6) covalent crosslinks or (7) a combination of the above interactions (Guan et al., 2017).

Hydrogels provide ideal 'soft material' systems to mimic the native microenvironments of the extra-cellular matrix due to their biocompatibility, mechanical and degradation properties (Geckil et al., 2010; Tibbitt & Anseth, 2009).

Furthermore, they are able to easily incorporate bioactive signals or other biomolecular structures such as nucleic acids, fatty acids, glycans and growth factors to form biomimetic scaffolds (Prince & Kumacheva, 2019).

The use of hydrogels as artificial extracullar matrices can prove particularly advantageous since they provide a three-dimensional environment similar to that present *in vivo* and can be modified to adapt to specific research needs. This can be particularly useful for studying the development of neural networks, as well as for applications in neural tissue engineering and regenerative medicine.

Given their properties and versatile fabrication, hydrogels have been applied in a wide range of biomedical and engineering applications including tissue engineering and regenerative medicine.

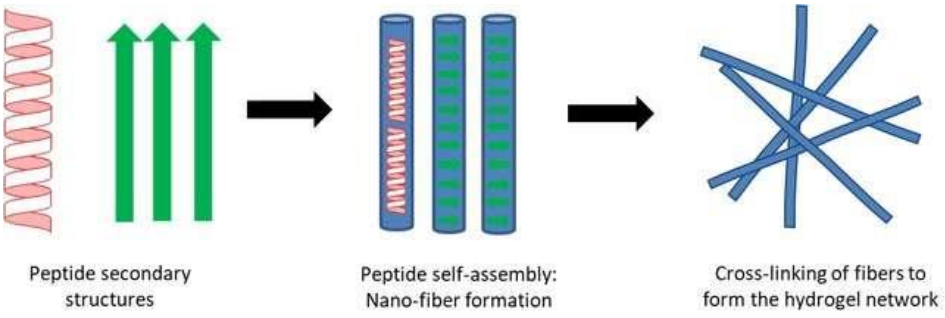

Figure 1.5 Scheme of the hydrogel self-assembly process

1.2.1.2 Chitosan

After cellulose, chitin is certainly one of the most abundant biopolymers in nature, being one of the main components of the exoskeleton of crustaceans but also the main constituent of the cell wall in arthropods and fungi.

From a chemical point of view it is a polysaccharide made up of several units of acetylglucosamine (more specifically, N-acetyl-D-glucos-2-amine) linked together with a β-1,4 type bond, the same as glucose units that make up cellulose. It is structurally identical to cellulose with the replacement of each hydroxyl group on each monomer with an amide group (Figure 1.6(a)).

The workability of chitin and its use are severely limited due to its poor solubility in aqueous solutions and in many organic solvents due to its high degree of crystallinity (Hirano, 1996). To be used conveniently in the biomedical and pharmaceutical fields, after extraction, it must be transformed into its deacetylated form through the use of sodium or potassium hydroxide: chitosan (Figure 1.6 (b)) (No & Meyers, 1995).

During the deacetylation process, the acetyl group (-COCH3) present in chitin gives way to the amino group (−NH2) in chitosan. The degree of deacetylation is defined as the number of amino groups along the chain: to consider it chitosan, a chitin must have a degree of deacetylation greater than 60%. The different types of chitosan can therefore be defined on the basis of the degree of deacetylation and the source of origin.

The molecular weight of chitosan (Molecular Weight, MW) is an important classification parameter which has been agreed into three different classes based on the MW: Low-Molecular-Weight (LMW), Medium-Molecular-Weight (MMW) and High- Molecular Weight (HMW).

In the world several million tons of chitin are collected every year, the easy availability combined with the low cost of the material, make chitosan of great interest also for a possible industrial "scale up" of the discoveries developed in the field of basic research.

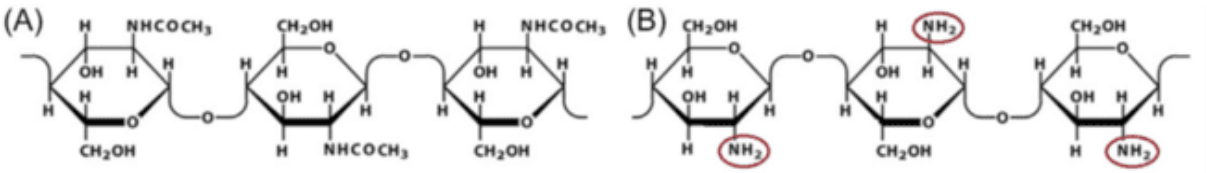

Figures 1.6 Chemical structure of chitin (A) and chitosan (B)

Properties of chitosan

The degree of deacetylation (DD) obtained, following the processing of chitin, influences the properties of chitosan. DD is the factor influencing the physical, chemical, and biological characteristics of chitosan (Rodríguez-Vázquez et al., 2015).

The solubility of chitosan depends on the distribution of the free amino and N-acetyl groups: at pH < 6.5 (acidic solutions) the free amino groups are protonated and confer a polycationic behavior and the molecule becomes soluble; at pH ⩾6.5 the amino groups tend to deprotonate, and the chitosan solution becomes insoluble in water (Kim et al., 2008).

Chitosan is an excellent candidate for biomedical applications as it is characterized by low toxicity, bioactivity and mucoadhesive properties, as well as having strong antibacterial properties in the low molecular weight formulation (Bano et al., 2017). Furthermore, this copolymer has the characteristics of being biodegradable, biocompatible, and soluble in aqueous solution. Biocompatibility itself depends on the degree of deacetylation: it has been shown that the higher the DD, the higher the bioaffinity of the material (Prasitsilp et al., 2000).

The surface of this biomaterial is positively charged and hydrophilic, which promotes cell adhesion, proliferation and differentiation (Figure 1.7) (Mota et al., 2012). More specifically, the use of chitosan has been demonstrated as an adhesion factor and scaffold for both 2D and 3D neuronal cultures (Di Lisa et al., 2020).

For all these properties, the use of chitosan has increased dramatically in tissue engineering and regenerative medicine in the last twenty years (Victor et al., 2020). The use of chitosan as a biomaterial has been approved by the Food and Drug Administration (FDA) for applications in biomedical devices, specifically in drug delivery and tissue engineering, with the aim of restoring the functionality of damaged tissues (De Masi et al., 2019).

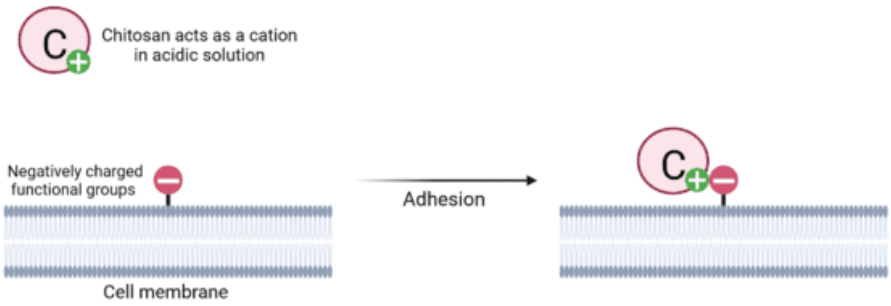

Figure 1.7 Cell membrane-chitosan adhesion process

1.2.2 Spontaneous Neuronal Activity in Vitro

The action potential (Figure 1.8) is the fundamental event of the electrical activity of neurons, represented by rapid changes in the membrane potential lasting a total of about 2 milliseconds. This electrical impulse plays a fundamental role in cellular communication, it is a stereotyped event capable of carrying messages even over long distances by being transmitted from one cell to another. Each action potential is therefore an alteration of the resting membrane potential (-70mV for neurons) and different phases can be identified:

- Depolarization: following a stimulus, the voltage-gated sodium channels are opened, and the membrane potential rises up to a threshold value of about -55mV. Any stimulus that is unable to exceed this threshold value will not generate any action potential. Once the threshold is exceeded, the opening of other sodium channels follows with the achievement of a membrane potential of +40mV.

- Repolarization: once the depolarization peak is reached, the permeability for sodium decreases while that for potassium increases, repolarizing the membrane towards negative values.

- Hyperpolarization: the repolarization carried out by the potassium channels is not hindered by those for sodium which are currently closed, this means that the membrane potential settles at the value of that of potassium of about 90mV. With the decrease of the permeability for sodium, the sodium-potassium pump, through the consumption of ATP, restores the potential bringing it back to that in resting conditions.

When neurons begin to develop synaptic connections, functional circuits are also established, leading to the production of spontaneous network-driven events involving large neuronal populations.

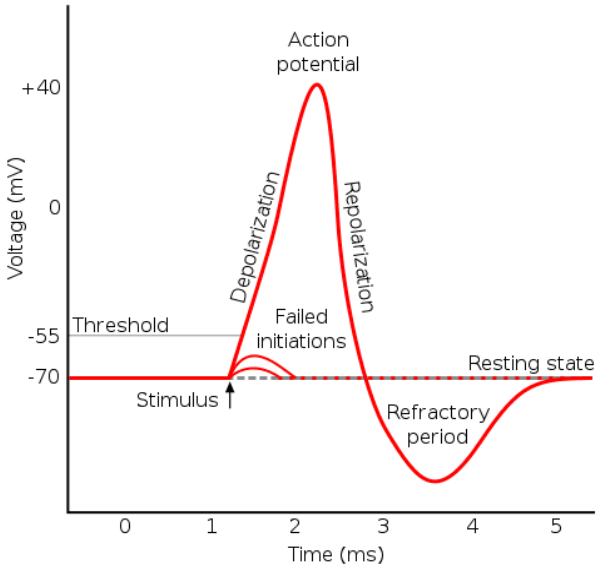

Figure 1.8 Schematic representation of a neuronal action potential

Neurons cultured in vitro also form networks giving rise to spontaneous electrical activity (Chiappalone et al., 2006). This activity can take on a different nature and changes as the network matures:

- **Spiking:** in the first week of culture there will be activity in the form of spikes, i.e. the action potentials of single cells, not correlated to each other, presenting various irregular firing frequencies.
- **Bursting:** starting from the second, the spikes will tend to group in bursts consisting of a rapid sequence of at least five spikes close together over time (Figure 1.9). Each burst can last from hundreds of milliseconds to even seconds.
- **Network burst:** Network activity expressed by network bursts occurs only in networks that have reached maturity, estimated at about 28 days in culture for 2D models (Tukker et al., 2016). Synchronized burst activity is a collective production encompassing the entire network of closely spaced action potentials, forming synchronous burst events interspersed with quiet periods with very little or no spikes. The collective network burst activity is important for cognitive processes and has been found in vivo during sleep.

It is commonly accepted that, to investigate and understand neural code, it is necessary to primarily focus on electrical activity based on groups of spikes or bursts (Marom & Shahaf, 2002). They are generated by a single neuron or a population of synchronously firing neurons

and form and change during development in a dynamic and experiential way (Quartz & Sejnowski, 1997).

The number and morphology of spike and burst signals change with the age of the network (Chiappalone et al., 2006).

Another component that acts on neuronal activity is the presence or absence of astrocytes. They play an important role in the regulation of neuron development and have also been shown to enhance the development of neuronal networks and action potentials in human iPSC-derived co-cultures (Tang et al., 2013). The addition of astrocytes to the neuronal model (Amiri et al., 2013) has also been reported to increase the synchronicity of networks. Furthermore, the inclusion of astrocytes also adds specific and physiologically relevant targets for toxic or non-toxic interactions with the culture that would not be present in a pure neuronal model.

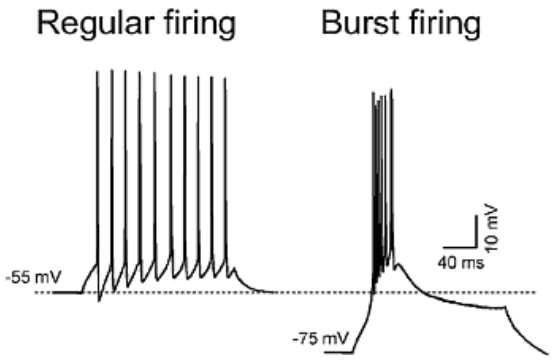

Figure 1.9 Comparison between spiking activity and bursting activity

Chapter 2

2. Data Analysis Tool

The purpose of this section is to describe the analysis algorithms employed for the realization of this thesis work, with the final aim of analyzing the data collected during the experiments.

1.3.1 Spycodes

The introduction of devices for multichannel recordings (such as Micro Electrode Arrays, MEA) has allowed to study the neural interdependence and the computational properties of dynamically interacting groups of cells (Miller & Wilson, 2008) and to monitor the electrophysiological activity of a cell population for a long time period (Bologna et al., 2010; Chiappalone et al., 2006).

Unfortunately, until 2010, the user was not given the ability to quickly perform a multi-channel analysis on more than one recorded file at a time. Commercial software tended to have only limited ability to incorporate new tools or modify existing ones. Some researchers started developing custom tools capable of analyzing data recorded on multiple electrodes, such as Mea Tools (Egert et al., 2002), Mea Bench (D. Wagenaar et al., 2005) and BSMART (Cui et al., 2008), but these tools did not provide a great variety of data analysis and did not allow to manage several data files in parallel.

The DIBRIS and IIT research groups, to solve these problems, have developed a new software package: SPYCODE (Bologna et al., 2010)(Figure 2.1) which provides a working environment capable of performing efficient data management and processing, since it includes a rich set of signal analysis tools.

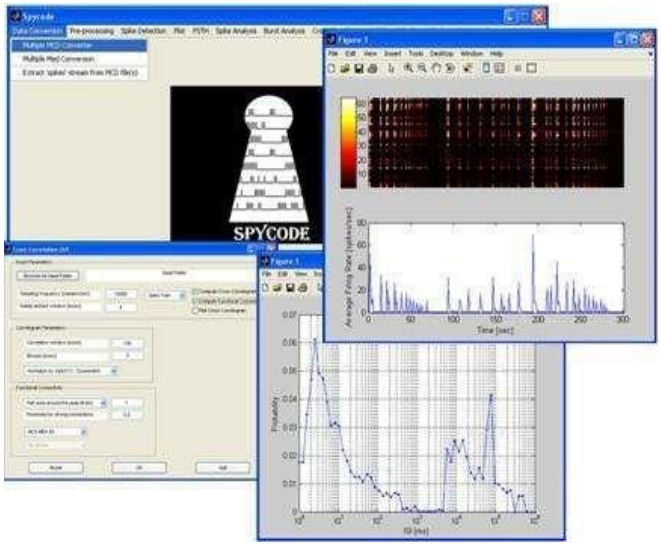

Figures 2.1 Running Spycode

A new type of analysis (Figure 2.2, 2.3) is achieved through information theory methods, connectivity map extraction, adaptive single-channel and group-channel burst detection methods, as well as classical algorithms and more common in neuroscience such as Spike Detection (automatic detection of action potential), Post Stimulus Time Histogram (histogram representing the average response of one or more cells in response to an external stimulus), Raster Plot (visual representation of the spike in the time), Mean Firing Rate (average firing rate over time), Inter Burst Interval (time interval between two consecutive bursts), etc.

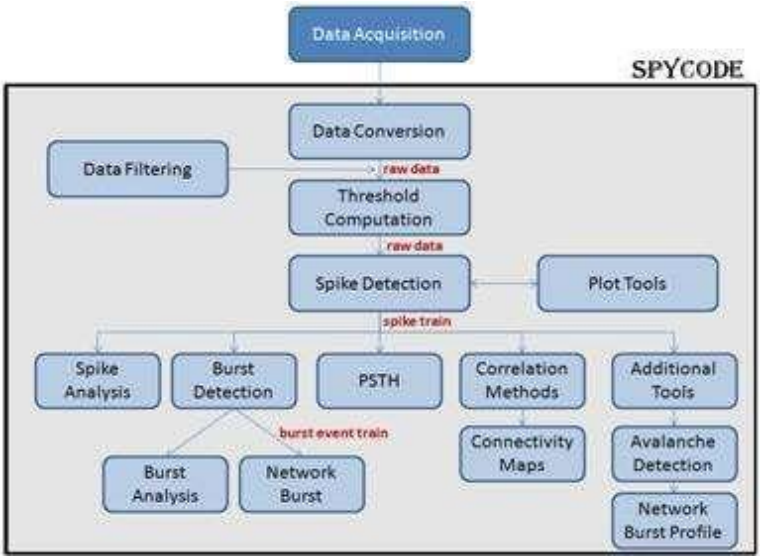

Figure 2.2 Scheme of the data analysis procedure implemented in Spycode.

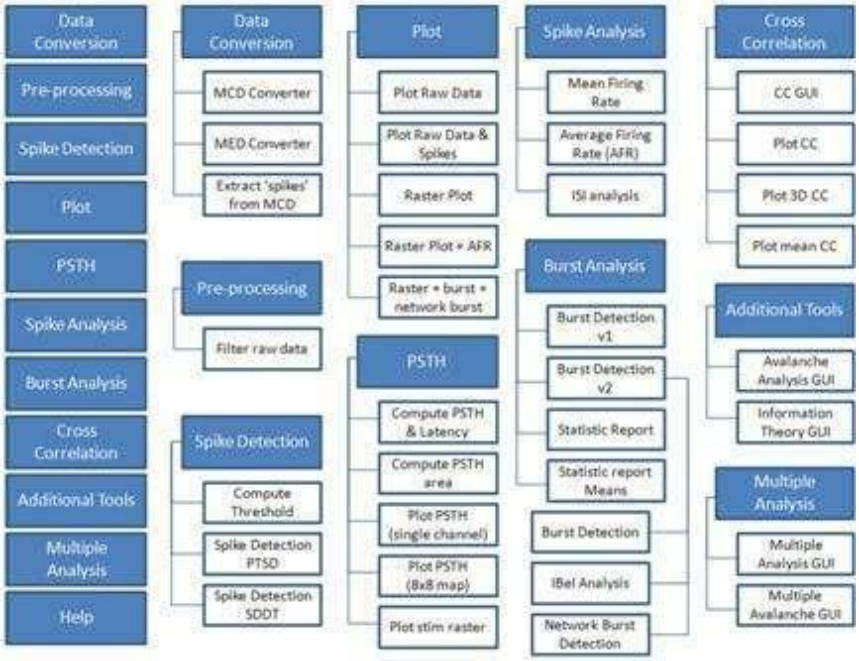

Figure 2.3 The complete structure of the Spycode MENU.

In the following, the analysis methods of this software that have been used to analyze the data of the experiments conducted for the aim of this thesis are presented.

They are divided into Spike Analysis, Burst Analysis and Raster Plot:

1.3.2 Spike Analysis

Signal filtering

The data was filtered using a Butterworth high-pass filter with a cut-off frequency of 200 Hz. This is necessary because the acquired data may contain low-frequency noise, such as background noise, work surface vibrations or interference from power lines. Applying a high pass filter removes this low frequency component, allowing you to focus on events of interest, such as spikes.

Spike Detection

The timing of the spikes is the first piece of information to be extracted from the raw data. Spikes are short voltage pulses with a duration of approximately 1-2 ms. Because typical signal-to-noise ratios are much greater than one, the most widely used method for identifying spikes is a threshold-based algorithm (Kamioka et al., 1996).

The single spike train is a time process (Spike Train, ST):

$$ST(t) = \sum_{S=1}^{N} \delta (t - t_S)$$

The equation reports the formal definition of a spike train, where t_s is the timing of a spike, N is the number of recognized spikes, and δ(t) is the Kronecker delta function.

It is important to consider stationarity, which plays a central role in neural signals. This is absent in experiments performed through non-implantable MEAs, both when recording spontaneous activity and when applying a stimulation protocol.

To identify a peak, you need to find, using the Calculate Thresholds command (Figure 2.4), the thresholds for the first recording step of each experiment.

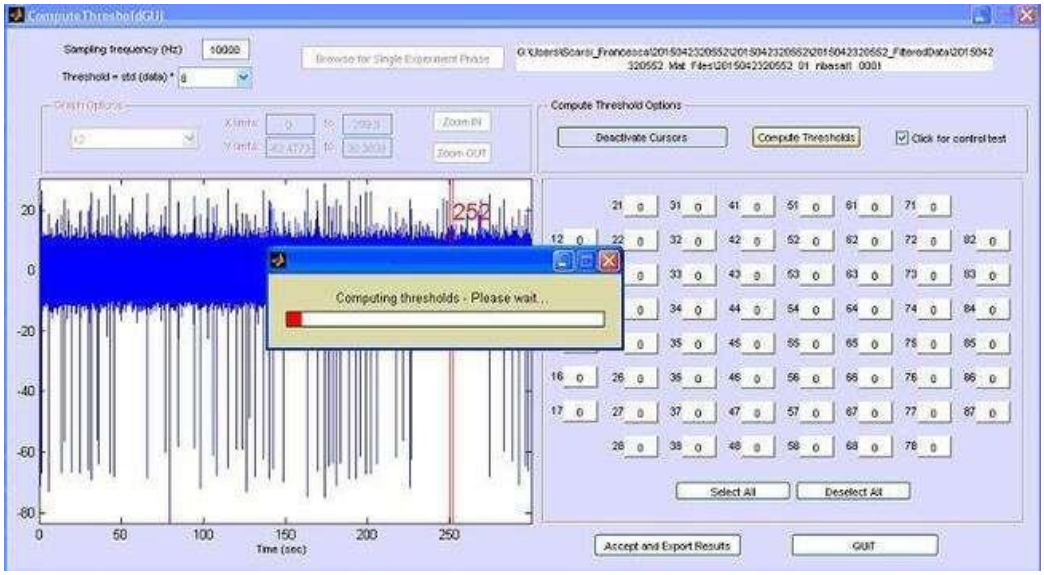

Figure 2.4 Threshold calculation interface

Once the thresholds are identified, a spike detection algorithm, called PSTD (Precise Timing Spike Detection) is applied to the neural signals (Maccione et al., 2009). It allows you to increase the accuracy of identifying the spike.

This algorithm requires three parameters: (1) the differential threshold, (2) the peak duration period, (3) the refractory period.

The differential threshold, set independently for each channel, is calculated based on the standard deviation of the noise signal. The algorithm calculates the maxima and minima of the

recorded voltage signal: when a minimum is found, it looks for the closest maximum with a window of width equal to the period of duration of the peak and vice versa. If the difference between the maximums and minimums found exceeds the differential threshold, the peak is identified and the instant in which it occurs is recorded. When the user decides to set the refractory period, all other maxima and minima with this time delay are not considered.

Firing Rate and Mean Firing Rate (MFR)

Once the spikes have been identified, the simplest and most direct way to characterize the activity level of a cell is to calculate its Firing Rate (Schneidman et al., 1998).

According to Adrian's definition (Wolbarsht, 1964), the firing frequency is the number of spikes over a fairly large time window with T representing the duration of the recording and N the number of spikes occurring at time t_s. If we count the peaks in a small window of dimensions Δt, centered on $(t_a - t_b)/2$ and divide by the width of the bin, we calculate the Instant Firing Rate (IFR).

In relation to MEAs, it is helpful to calculate the entire culture's FR or IFR and see how it changes based on the stimulation delivered. These quantities are obtained simply by calculating the FR and the IFR of each single channel and then averaging all the active electrodes of the MEA, obtaining the Mean Firing Rate (MFR) and the Average Firing Rate (AFR) of the network.

The MFR is a statistical indicator representing the number of spikes per unit of time. It can be defined as an averaged time estimate, calculating the rate between the number of spikes included in a time interval T and the same time interval T.

It is an important parameter because it determines the effective activity of the network channels and allows us to study the evolution of the behavior of the same in response to external influences.

Inter Spike Interval (ISI)

The interval between spikes (ISI) represents the time interval between two successive spikes. The ISI distribution is an estimate of the probability density function of the ISI and is a useful statistic for describing spike trains.

Mathematically it can be expressed with the following expression:

$$ISI(r) = \sum_{S=1}^{N-1} \delta (t_{S+1} - t_S - r)$$

Where N is the number of spikes, τ is the amplitude of the bin and s the time point of the spike S.

The presence of bursting activity in vitro usually leads to bimodal ISI histograms, where intra-burst ISI values are lower, while inter-burst ISI values are higher.

1.3.3 Burst Analysis

Definition of bursts

Bursts are one of the relevant electrophysiological phenomena in the analysis of neuronal activity, Bursts are important as they represent a highly coherent and synchronous form of activity among a group of neurons.

We can define the burst as a sequence of dense spike packets with a duration equal to the sum of the ISIs within the burst and separated by an interval called IBI (Inter Burst Interval), relatively long compared to the burst duration.

Finding bursts in electrophysiological activity can be useful for several purposes, for example, it can provide insight into the development and function of neural networks. Burst analysis can help understand how neurons organize and communicate with each other to form functional circuits.

This analysis may involve identifying the temporal patterns of the spikes, extracting parameters such as the frequency, duration, and amplitude of the bursts, and analyzing the spatio-temporal relationships between the neurons involved in the bursts.

Burst Detection

The algorithm (Pasquale et al., 2010)used to detect bursts evaluates the logISIH (Logarithmic Inter-Spike Interval Histogram) to look for the best threshold (ISIth) between intra-burst (i.e., within bursts) and inter-burst (i.e., between bursts) activity. bursts and/or out of bursts).

If the ISIth is less than 100ms, the algorithm uses the value of ISIth to determine the maximum ISI allowed within a burst.

Conversely, if ISIth is greater than 100ms, the algorithm uses two different thresholds: the first (100ms) is used to detect core bursts, while the second (ISIth) is used to extend core bursts to boundaries to include all peaks whose ISI is less than ISIth.

Mean Burst Rate (MBR)

The Mean Burst Rate provides information on the average number of bursts generated by neurons during a given time interval.

To calculate the Mean Burst Rate, the total number of bursts recorded during the time interval considered, in our case one minute, is counted and divided by the duration of that interval. The mean burst rate can be useful for evaluating the general activity of cultured neural networks. A high average burst rate may indicate higher synchronous activity and stronger communication between neurons. On the other hand, a lower average burst rate may suggest less synchronous activity and less coherent communication between neurons.

The mean burst rate can vary based on several factors, such as the maturity of the neuron cultures, the density of neurons on the array surface, and the experimental conditions. For example, more mature cultures of neurons tend to have a higher mean burst rate than less mature cultures, as neural networks have developed and stabilized synaptic connections.

Mean Burst Rate analysis can provide valuable information for understanding the dynamics of neural networks in vitro and can be used to compare different experimental conditions or treatments. [spikes/min]

Mean Burst Duration (MBD)

Mean Burst Duration provides information on the average duration of neuronal bursts, i.e., the time between the start and the end of a burst. To calculate the Mean Burst Duration, the duration of each individual burst is recorded during a given time interval and then the average of these durations is calculated.

Mean Burst Duration can be useful for assessing the temporal dynamics of neuronal activity. A longer average burst duration may indicate prolonged synchronous activity and greater persistence of the involved synaptic connections. On the other hand, a shorter average burst duration may suggest greater temporal variability in neuronal activity and less stable communication between neurons.

Mean Burst Duration, like Mean Burst Rate, can be influenced by several factors, such as the maturity of the neuron culture, the density of neurons on the array, and the experimental

conditions. In general, more mature cultures of neurons tend to have a longer mean burst duration than less mature cultures, since the neural networks are more developed and stable.

Mean burst duration analysis can provide valuable insights into the temporal dynamics of in vitro neural networks and can be used to compare different experimental conditions or treatments. [sec]

Random Spikes

The random spike rate provides information on the presence of neuronal spikes not associated with bursts or coherent patterns of activity.

To calculate the percentage of random spikes, the neuronal activity recorded by the electrodes during a given time interval is analyzed and the spikes that are not part of bursts or patterns of synchronous activity are identified. Next, the percentage of random spikes out of the total recorded spikes is calculated.

The percentage of random spikes can be useful to evaluate the presence of spontaneous and non-synchronous activity in the neural network. A high random spike rate indicates more random spikes, which could be attributed to uncorrelated neural events or recording noise. On the other hand, a lower random spike rate suggests a greater predominance of neuronal activity organized in bursts or patterns of coherent activity.

Analysis of the percentage of random spikes can provide insight into the stability and coherence of neuronal activity in cultured neurons. Furthermore, it can be useful to evaluate the effect of different treatments or experimental conditions on the occurrence of spontaneous and random activities. [% spikes]

Burst Index (BI)

Bursts come in different forms, so the number of bursts is not sufficient to describe the burstiness of a culture. It is essential to consider the size of the bursts and the aggregate number of peaks.

The BI(D. A. Wagenaar et al., 2006) it is an index ranging from 0 (no burst) to 1 (there are no spikes outside the bursts) defined mathematically as:

$$BI = \frac{f_{15} - 0.15}{0.85}$$

where f_{15} is the fraction of the total number of peaks represented by the 15% of the 1-second-long bins, into which the recording has been divided, with the highest count.

If the firing frequency is tonic, the f_{15} parameter will be close to 0.15, otherwise, if the recording has a pattern of burst activity f_{15} will be very close to 1, as most of the spike will be contained in the burst.

It must be emphasized that, unlike the parameters previously illustrated in the Burst Analysis section, the BI is obtained directly from the Spike Detection results and integrates the information of all channels into a single index for the entire crop.

Thus, BI reflects the portion of spikes within bursts and provides a more detailed illustration of burst structure, where higher BI values indicate an overall burst-dominated network and lower BI values indicate burst activity. more random spiking. [Index 0 to 1]

1.3.4 Raster Plots

The Raster Plot is a graphical representation that allows you to have a qualitative view of the activity of the neural network. It shows the spike trains recorded for each electrode as a function of time (Figure 2.5).

The information provided by these graphs is very important, as it allows us to carry out a first general qualitative evaluation of the experimental data. Observing the raster graph, for each phase, it is possible to identify the noisy channels to be eliminated for subsequent analyses.

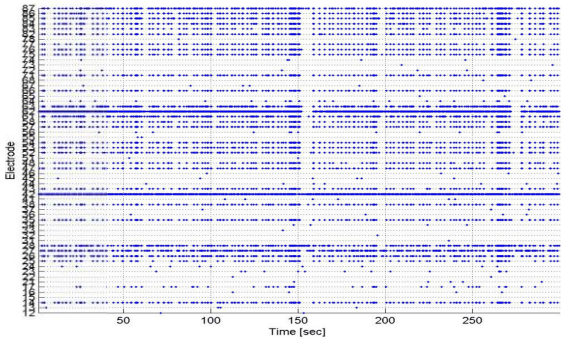

Figure 2.5 An example of a raster plot

Chapter 3

3. Materials and Experimental Methods

For this thesis I have prepared and electrophysiologically and morphologically characterized three different types of nerve cell cultures:

- The 2D cultures (Figure 3.1) were prepared on 2D MEA: the cells were plated on the surface of the MEA, previously treated with an adhesion factor, and recorded from its planar electrodes. Chitosan was used as an adhesion factor.

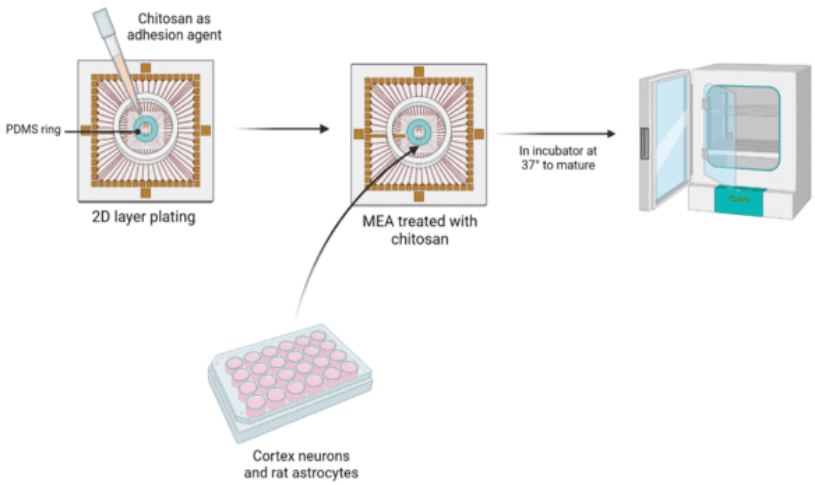

Figure 3.1 Schematic representation of 2D culture preparation

- The 3Don2D cultures (Figure 3.2) were prepared on 2D MEAs, starting from a 2D layer of neurons and subsequently depositing a three-dimensional layer of hydrogel containing neuronal cells on this two-dimensional layer. However, the neurons contained in the three-dimensional hydrogel layer are not directly recorded by the

MEAs, since only the bottom 2D layer is in contact with the electrodes. NeuroGlycoGel chitosan hydrogel is used as a scaffold.

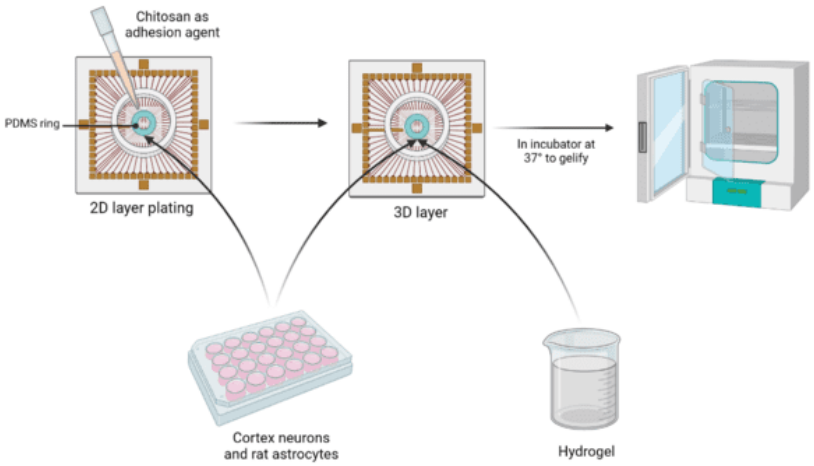

Figure 3.2 Schematic representation of 3Don2D culture preparation

- The 3D cultures (Figure 3.3) were prepared directly on 3D MEAs, only the activity of the hydrogel layer is captured as the electrodes of the 3D MEAs record from their tip. Again, NeuroGlycoGel chitosan hydrogel is used as a scaffold.

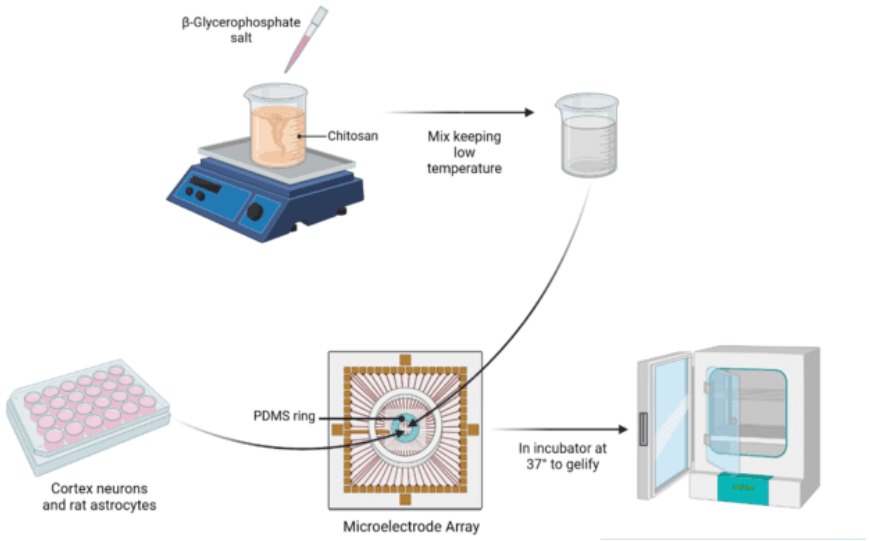

Figure 3.3 Schematic representation of 3D culture preparation

The purpose of this section is to expose in more detail the materials and protocols used both for the preparation of the cultures and for the subsequent analyses:

2.1 Culture of nerve cells

2.1.1 Culture of rat astrocytes

Frozen rat cortical astrocytes were used. Astrocytes were thawed and plated in a T-75 flask with DMEM High Glucose supplemented with 10% fetal bovine serum and 1% penicillin/streptomycin and incubated at 37°C with 5% CO2.

The medium was changed every 3 days for 7-10 days. On the day of plating, astrocytes were mixed with iN (1:1) in Neurobasal-iN 15

2.1.2 Cultures of human-derived induced pluripotent stem cells (hiPSCs)

Fibroblasts were obtained from a healthy donor and hiPSCs were generated by lentiviral transduction, with reprogramming factors cMYC, SOX2, OCT4 and KLF4.

Subsequently, two other lentiviral vectors were used to generate an rtTA/NgN2-positive hiPSCs line. The cells were provided by Frega et al. and were supplied in frozen vials.

After rapid thawing, the cells were plated in six well plates pre-coated with MATRIGEL. Pluripotency was maintained in Essential 8 Flex Medium (Thermo Fisher Scientific) supplemented with 1% pen/strept, i50 ug/ml G418, and 0.5 ug/ml puromycin (E8F).

The medium was changed every 2 days and the cells were subdivided twice a week using ReleSR reagent (ReLeSR, Stem Cell Technologies) and supplementing the medium with Revitacell for the next 24 hours. Samples were maintained in a 37°C 5.5% CO2 incubator.

2.1.3 Differentiation of hIPSCs into excitatory neurons

Due to the uniqueness of the rtTa/Ngn2 positive hIPSCs line, layer 2/3 excitatory cortical neurons were generated by overexpressing the neuronal determinant Neurogenin 2 (NgN2) upon doxycycline treatment.

Then, hiPSCs were detached using an enzyme mix and plated as single cells on 6-well plates with E8F medium with 4 ug/ml doxycycline to initiate differentiation. This step is defined as Day After Differentiation 0 (DAD 0).

The next day, the medium was replaced with 100x N2 supplement supplemented DMEM/F12; 100x MEM non-essential amino acid solution, 1% pen/strep, human BDNF (10ug/ml), human

NT-3 (10ug/ml,), and doxycycline (4ug/ml). At this stage the cells are no longer pluripotent and can be considered as an early stage of induced neurons (iN).

At DAD 3, neurons were detached using an enzyme mix and suspended in neurobasal medium) supplemented with 1% pen/strept, 50X B-27, 100X glutaMAX, human BDNF (10ug/ml, human NT-3 (10ug/ml) and doxycycline (4ug/ml) (we will refer to this culture medium as NeuroBasal-iN).

After centrifugation, the cell pellet was resuspended in 2 mL of NeuroBasal-iN and the cells were then used for experiments.

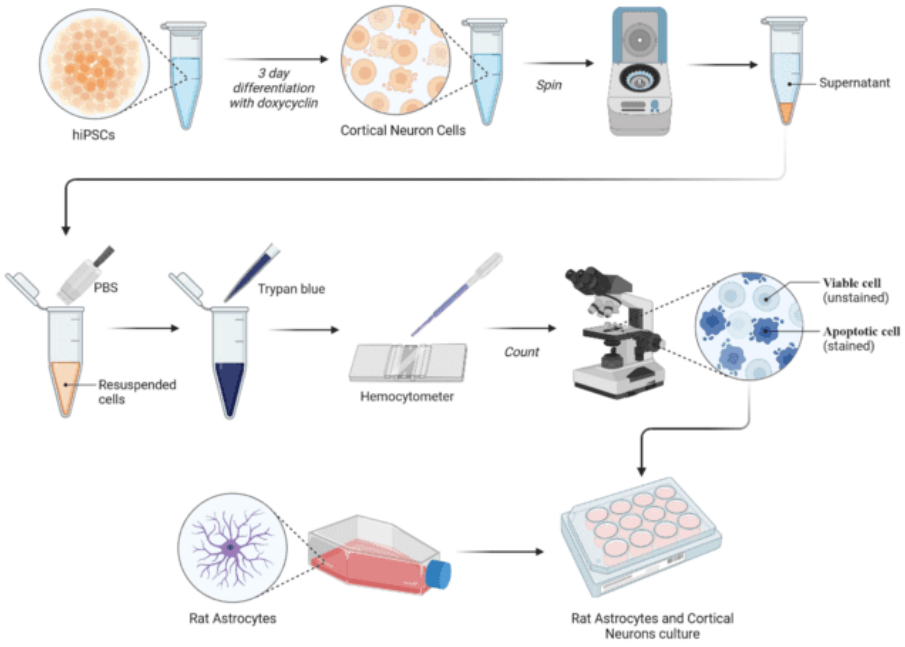

Figure 3.4 Schematic representation of cell differentiation and counting

2.1.4 Preparation of the NeuroGlycoGel chitosan hydrogel

NeuroGlycoGel consists of two components: the main chitosan-based solution and the crosslinking solution. Both components are supplied in the form of powders.

The main solution is obtained by dissolving the powder in buffer dissolution, leaving it under stirring on a magnetic stirrer overnight.

The crosslinking solution is prepared by dissolving the powder directly in the culture medium.

The solutions are sterilized before being used with the cells. The main solution is autoclaved at 120°C for 20 minutes, while the crosslinking solution is filtered with a 0.22 µm syringe filter.

NeuroGlycoGel is prepared by adding the crosslinking solution dropwise to the main component. The two solutions are mixed for 15 minutes keeping them at a temperature of about 4°C to prevent the gelling process from starting.

2.1.5 Preparation protocol for 2D, 3D and 3Don2D neuronal cultures

The cultures were prepared on MEA delimiting the active area of the electrodes using a ring of PDMS (polydimethylsiloxane).

MEAs were washed using a 5% soap and deionized water solution. Subsequently they were washed with simple deionized water, dried using nitrogen and finally sterilized in an oven for 3 hours at a temperature of 120°C.

A 1% w/v chitosan solution in 0.1M acetic acid was used as an adhesion factor. The chitosan solution was autoclaved at 120°C, 1atm, for 20 minutes. Functionalization of MEAs was achieved by depositing a 60 µl drop of chitosan solution on the surface of each matrix. The deposition of the cells took place by exploiting the PDMS ring to contain the plating area, so as to reach the desired cell concentration (2500 cells/$mm^{2)}$ in correspondence with the electrode area. The matrices were incubated overnight in an incubator and the excess solution was removed with a pipette before performing two washings with deionized water and one normalization with culture medium.

The 3D and 3Dsu2D cultures were prepared using NeuroGlycoGel as thermosensitive hydrogel, in which neurons co-cultured with astrocytes were encapsulated. The cell density used in each sample was defined as 1 million per scaffold with 30% astrocytes; 20 µl of this cell-gel solution were deposited in the PDMS rings of each MEA. Finally, the MEAs were placed in an incubator at 37° for 45 min to trigger the gelation process, and the Neurobasal culture medium was added.

2.2 Electrophysiology experiments for functional characterization

2.2.1 Recording setup

The experimental set-up used for data logging included:

- MEA microelectrode array
- Integrated preamplifier
- MC Card capture card
- MCRack software, capable of displaying and recording signal progress online
- Chamber heated and containing 20% O2, 75%N2 and 5% CO2, in order to simulate the conditions in an incubator.
- Thermostat

MEA

MEA consists of a planar array of microelectrodes manufactured by Multi Channel System (MCS, Reutlingen, Germany) and is a compact technology born in the late 1970s for in vitro experiments with brain and muscle cells. It is biocompatible, durable, and each electrode has a reasonably low impedance (less than 500k Ω at 1Hz) to allow for the detection of small extracellular signals (10 to 100 μV).

The low impedance also allows sufficient stimulation current to be passed without exceeding the electrochemical breakdown voltage of the water and other components of the culture medium (usually about 1V) (Potter, 2001). The surface of the MEA and the leads of the electrodes are coated with a biocompatible insulator (usually polyamide or nitride/silicon oxide) which prevents electrical shorting with the culture medium and allows cell adhesion after coating with the substrate. traditional cell culture.

There are several types of MEAs which differ in the diameter and the distance between the electrodes. The most used is the MEA 60: it is composed of 60 planar electrodes of circular shape made of low impedance titanium nitride (TiN). The electrical contacts are made of titanium and the insulating parts of silicon nitride. The 60 electrodes are arranged in different layouts.

Two types of MEAs were used for this work:

- 2D MEAs (Figure 3.5) are the most common and have been used to measure the activity of 2D and 3D cultures on 2D; they are composed of a square matrix of (8x8) electrodes in TiN (titanium nitride), for a total of 60 electrodes. One of these electrodes is connected to ground and acts as a ground electrode (the number 15), thus bringing the number of measurable electrodes to 59. Silicon nitride (SiN) is used as an insulator. These 60 electrodes have a diameter of 30 μm and are 200 μm apart and being flat, they only measure the activity of the surface layer resting on them. A large number of electrodes is necessary to observe the behavior of multiple neurons simultaneously, which becomes particularly relevant for mature cultures.

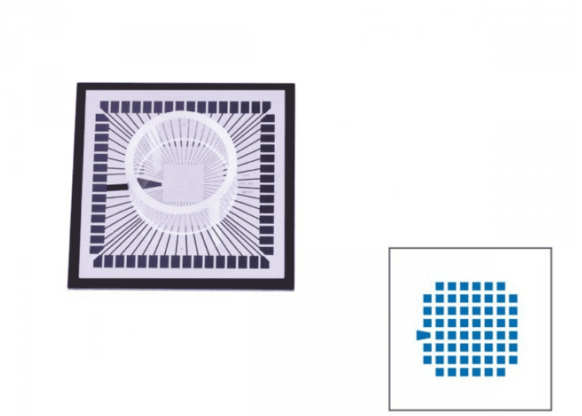

Figure 3.5 2D 8x8 MEA matrix, 60 channels

- The 3D MEAs (Figure 3.6) are of new production and have been used to measure the activity of the 3D cultures, they differ from the 2D MEAs in the shape of their electrodes which, being needle-like, penetrate the hydrogel and allow to measure the activity of an inner layer of the culture, however these electrodes only measure from their tip so they are unable to measure layers at different depths than that to which the electrode tip penetrates. In our case, MEAs with 60 electrodes of 100 microns depth were used.

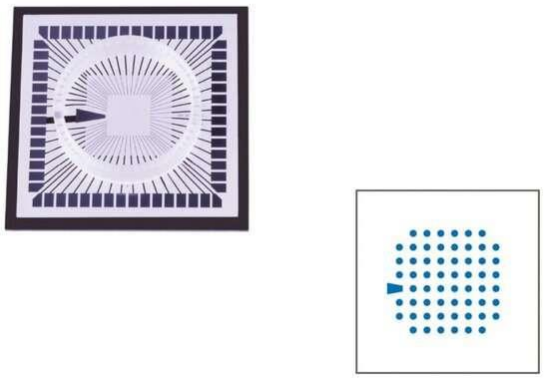

Figure 3.6 8x8, 60-channel 3D MEA matrix

One of the advantages of MEAs compared to other methods of electrophysiological investigation lies in the fact that they can keep neurons alive for several weeks: to allow this, the culture is immersed in a medium with all the necessary nutrients thanks to a ring of glass, 6 mm high, placed around the array.

The culture is usually covered with an airtight polydimethylsiloxane (PDMS) lid (Figure 3.7). PDMS is a biocompatible, transparent polymer that can be molded into specific shapes and possesses useful properties, such as permeability to gases (e.g., CO2, which is required to maintain stable pH conditions) and impermeability to water vapour, thus reducing evaporation and therefore the osmolarity variations of the medium. In addition, it provides a physical barrier that largely prevents the entry of airborne pathogens.

Figure 3.7 Polydimethylsiloxane PDMS lids.

Amplifier

The amplification stage (Figure 3.8) developed specifically for MEAs has made it possible to solve some fundamental problems, such as the reduction of the cables necessary to connect 60 electrodes simultaneously and the elimination of interference between the different channels due to crosstalk phenomena.

The amplifier used in this thesis is an integrated device containing a preamplifier stage and a filter stage for each of the 60 channels.

The MEA array is positioned in the center of the device and interfaced by rows of needle connectors. The design is compact and thanks to the SMD (surface-mounted) technology of the pre-amplifiers and pre-filters, the entire hardware, the complete circuit, and the amplifier have been built in a single housing ensuring an excellent signal-to-noise ratio during the registration phase.

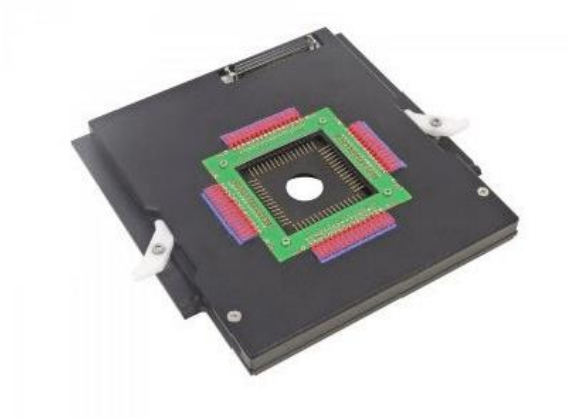

Figure 3.8 Amplifier for MEA

MC Card

For the acquisition and recording of the signals coming from the micro-electrode matrix, an acquisition card and software for the real time visualization of the electrophysiological signals (MCRack) were used. The MC Card acquisition card (Figure 3.9) is equipped with an A/D converter that allows you to record signals from 128 channels, sampled at a maximum

frequency of 50 kHz and 12-bit resolution. The sampling rate and the gain are selectable by the software, being able to vary within a range of values between ±4V and ±400mV.

Figure 3.1 MC Card

MCRack

MC Rack (Figure 3.10) is an acquisition software supplied by Multichannel Systems for recording data from multichannel cards. The time windows of the signal of all 60 electrodes are displayed on the monitor, allowing the progress of the signals to be monitored online, even during the recording phase.

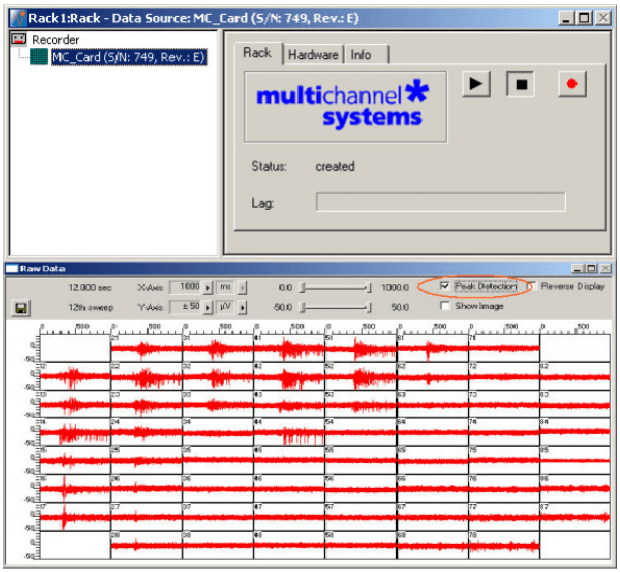

Figure 3.2 MCRack

Atmospheric control

To minimize the cellular stress due to leaving the incubator, an attempt was made to replicate its microenvironment by controlling parameters such as temperature and CO2 concentration in the MEA recording area.

For atmospheric control, a chamber was designed which, through small tubes, receives a constant flow of a mixture of 5% CO2, 20% O2 and 75% N2, keeping the cells in optimal conditions (pH ≈ 7.4 and osmolarity ≈ 230 mOsm).

Thermostat

All MEA detections were carried out at a temperature of 37.0°C, optimal for the growth of cultured cells and for a good response to stimuli. Connected to the amplification base, a small thermostat (Figure 3.11) allowed to maintain the desired temperature on the support plate of the MEAs.

Figure 3.11 Thermostat

2.2.3 Registration protocol

The recording sessions took place:

- For 2D cultures at: 21DIV, 26-28DIV, 32-34DIV, 37-41DIV (Figure 3.12).

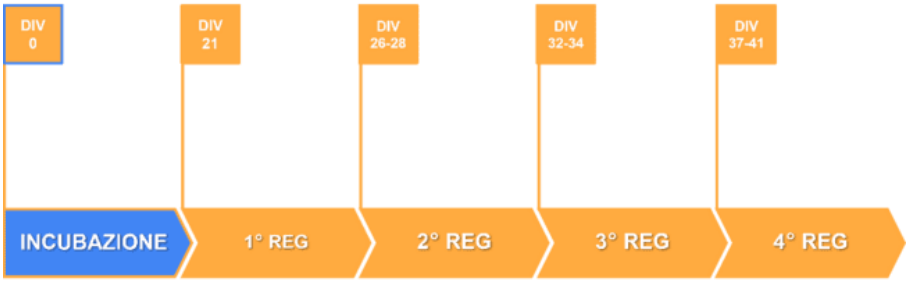

Figure 3.12 Recording sessions for 2D cultures

- For 3Don2D cultures at: 31DIV, 39DIV, 46DIV, 53DIV, 60DIV, 67DIV, 70DIV, 73DIV (Figure 3.13).

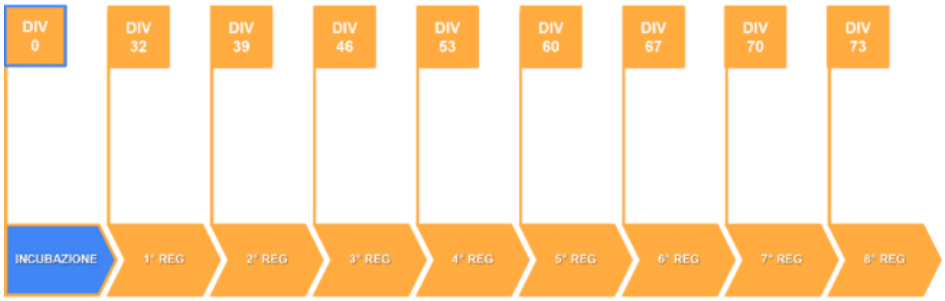

Figure 3.13 Recording sessions for 3Don2D crops

- For 3D crops at: 27DIV, 32DIV, 39DIV, 46DIV, 53DIV, 60DIV, 67DIV, 74DIV, 81DIV, 88DIV, 95DIV, 99DIV, 102DIV, 109DIV (Figure 3.14).

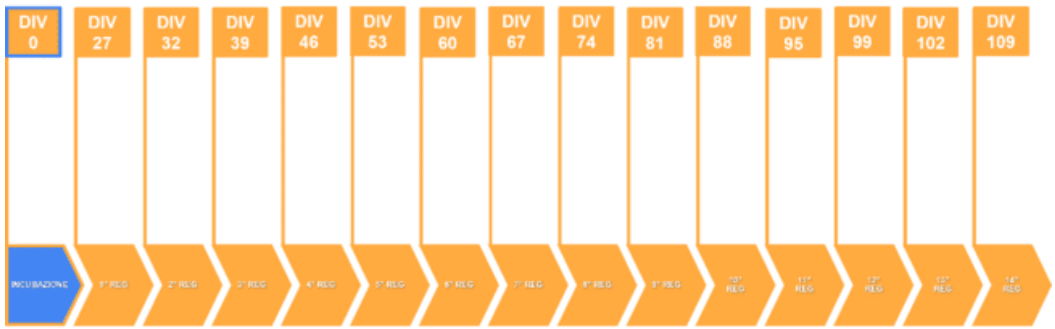

Figure 3.14 Recording sessions for 3D crops

In each recording session the instruments mentioned in the previous chapters were used and only after obtaining the data was a partial change of the culture medium carried out, removing 0.6 ml with a pipette and inserting fresh 0.8 ml.

The modus operandi followed for all acquisitions is as follows:

- 5 minutes adaptation (37°C, 5% [CO2], humidity [85-95] %)
- 10 minute electrophysiological activity recording (37°C, 5% [CO2], humidity [85-95]%)

The collected data were subsequently analyzed using the algorithms described in the state of the art.

2.2.4 Database and data organization

The data collected during the experiments were organized in an Excel database (Figure 3.15) to allow a quick visualization of the aspects that characterized each of them.

The main fields of interest are:

- Experiment file name: each experiment has a name, this is a string that contains information about the experiment that was performed and the MEA ID;
- DIV: identifies the number of days in vitro;
- Date: is the date on which the experiment was performed;
- MEA ID: the identification code of the MEA used;
- MEA type: identifies the type of MEA used;
- Electrodes excluded: electrodes excluded from the recording because they are noisy;
- Culture quality: it is an evaluation of the activity of the culture. The appreciation relates to the network performance observed while running the experiment.

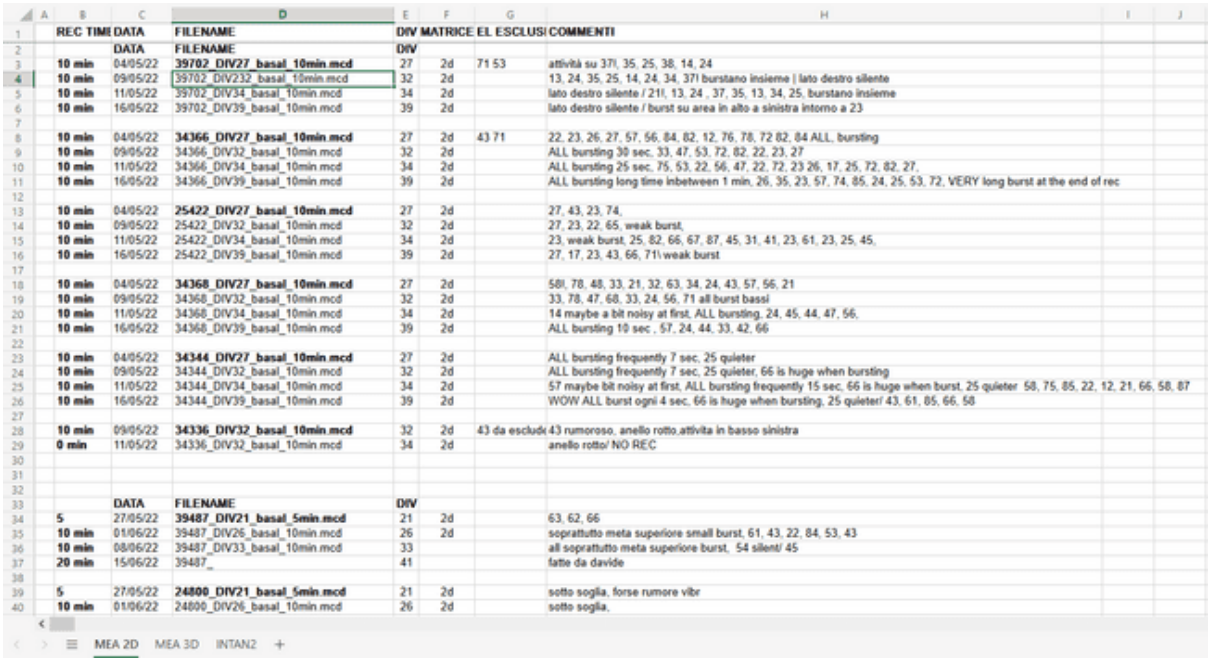

	REC TIME	DATA	FILENAME	DIV	MATRICE	EL ESCLUSI	COMMENTI
		DATA	FILENAME	DIV			
	10 min	04/05/22	39702_DIV27_basal_10min.mcd	27	2d	71 53	attività su 37\ 35, 25, 38, 14, 24
	10 min	09/05/22	39702_DIV232_basal_10min.mcd	32	2d		13, 24, 35, 25, 14, 24, 34, 37\ burstano insieme \ lato destro silente
	10 min	11/05/22	39702_DIV34_basal_10min.mcd	34	2d		lato destro silente / 21\ 13, 24 , 37, 35, 13, 34, 25, burstano insieme
	10 min	16/05/22	39702_DIV39_basal_10min.mcd	39	2d		lato destro silente / burst su area in alto a sinistra intorno a 23
	10 min	04/05/22	34366_DIV27_basal_10min.mcd	27	2d	43 71	22, 23, 26, 27, 57, 56, 84, 82, 12, 76, 78, 72 82, 84 ALL, bursting
	10 min	09/05/22	34366_DIV32_basal_10min.mcd	32	2d		ALL bursting 30 sec, 33, 47, 53, 72, 82, 22, 23, 27
	10 min	11/05/22	34366_DIV34_basal_10min.mcd	34	2d		ALL bursting 25 sec, 75, 53, 22, 56, 47, 22, 72, 23 26, 17, 25, 72, 82, 27,
	10 min	16/05/22	34366_DIV39_basal_10min.mcd	39	2d		ALL bursting long time inbetween 1 min, 26, 35, 23, 57, 74, 85, 24, 25, 53, 72, VERY long burst at the end of rec
	10 min	04/05/22	25422_DIV27_basal_10min.mcd	27	2d		27, 43, 23, 74,
	10 min	09/05/22	25422_DIV32_basal_10min.mcd	32	2d		27, 23, 22, 65, weak burst,
	10 min	11/05/22	25422_DIV34_basal_10min.mcd	34	2d		23, weak burst, 25, 82, 66, 67, 87, 45, 31, 41, 23, 61, 23, 25, 45,
	10 min	16/05/22	25422_DIV39_basal_10min.mcd	39	2d		27, 17, 23, 43, 66, 71\ weak burst
	10 min	04/05/22	34368_DIV27_basal_10min.mcd	27	2d		58\ 78, 48, 33, 21, 32, 63, 34, 24, 43, 57, 56, 21
	10 min	09/05/22	34368_DIV32_basal_10min.mcd	32	2d		33, 78, 47, 68, 33, 24, 56, 71 all burst bassi
	10 min	11/05/22	34368_DIV34_basal_10min.mcd	34	2d		14 maybe a bit noisy at first, ALL bursting, 24, 45, 44, 47, 56,
	10 min	16/05/22	34368_DIV39_basal_10min.mcd	39	2d		ALL bursting 10 sec , 57, 24, 44, 33, 42, 66
	10 min	04/05/22	34344_DIV27_basal_10min.mcd	27	2d		ALL bursting frequently 7 sec, 25 quieter
	10 min	09/05/22	34344_DIV32_basal_10min.mcd	32	2d		ALL bursting frequently 7 sec, 25 quieter, 66 is huge when bursting
	10 min	11/05/22	34344_DIV34_basal_10min.mcd	34	2d		57 maybe bit noisy at first, ALL bursting frequently 15 sec, 66 is huge when burst, 25 quieter 58, 75, 85, 22, 12, 21, 66, 58, 87
	10 min	16/05/22	34344_DIV39_basal_10min.mcd	39	2d		WOW ALL burst ogni 4 sec, 66 is huge when bursting, 25 quieter/ 43, 61, 85, 66, 58
	10 min	09/05/22	34336_DIV32_basal_10min.mcd	32	2d	43 da esclud	43 rumoroso, anello rotto,attivita in basso sinistra
	0 min	11/05/22	34336_DIV32_basal_10min.mcd	34	2d		anello rotto/ NO REC
		DATA	FILENAME	DIV			
	5	27/05/22	39487_DIV21_basal_5min.mcd	21	2d		63, 62, 66
	10 min	01/06/22	39487_DIV26_basal_10min.mcd	26	2d		soprattutto meta superiore small burst, 61, 43, 22, 84, 53, 43
	10 min	08/06/22	39487_DIV33_basal_10min.mcd	33			all soprattutto meta superiore burst, 54 silent/ 45
	20 min	15/06/22	39487_	41			fatte da davide
	5	27/05/22	24800_DIV21_basal_5min.mcd	21	2d		sotto soglia, forse rumore vibr
	10 min	01/06/22	24800_DIV26_basal_10min.mcd	26	2d		sotto soglia,

MEA 2D MEA 3D INTAN2 +

Figures 3.3 Database screenshot

2.3 Imaging experiments for morphological characterization

2.3.1 Fluorescence microscope

The fluorescence images were acquired using an Olympus BX-51 microscope, with a Hamamatsu Orca ER II cooled CCD camera (Figure 3.16) by means of the ImageJ ProPlus software (Media Cybernetic).

Figure 3.16 Olympus BX-51 microscope, with Hamamatsu Orca ER II cooled CCD camera

2.3.2 Immunofluorescence technique

The immunofluorescence technique was used to evaluate the morphology of the culture at the end of the experiment (Figure 3.17). This technique is used to highlight some cellular components, thus allowing them to be visualized and evaluated under a microscope.

More precisely, in the components to be highlighted, the presence of particular antigens is sought using the respective antibodies, which, made fluorescent by a fluorophore, respond to the absorption of photons by exhibiting fluorescence at different wavelengths. The difference between the different fluorophores that can be used is given by the different absorption and emission spectrums.

The cultures were washed with PBS prewarmed to 37°C and then fixed with 4% paraformaldehyde (PFA) for 15 minutes at room temperature. Once the PFA was removed and

two washings in PBS were performed, Triton-X was applied in a concentration of 0.3% diluted in PBS for 10 minutes, with the aim of increasing cell permeabilization.

The non-specific binding of the antibodies was blocked by incubation for 45 minutes in a buffer solution "Blocking Buffer" consisting of PBS, 0.3% BSA (bovine serum albumin) and 0.5% FBS (bovine serum fetal).

The cultures were labeled with primary antibodies: Tubulin βIII (1:500, dendritic microtubule associated protein), GFAP (1:500, glial fibrillar acid protein associated), diluted in Blocking Buffer for 2 hours at room temperature.

Subsequently they were washed three times with PBS and finally exposed to the secondary antibody: Alexa Fluor 488, Goat anti rabbit, diluted 1:700, Goat anti mouse diluted 1:1000. Finally, the samples were exposed to Dapi 1:10000 (nuclei marker that binds to AT-rich regions of DNA) for 10 min.

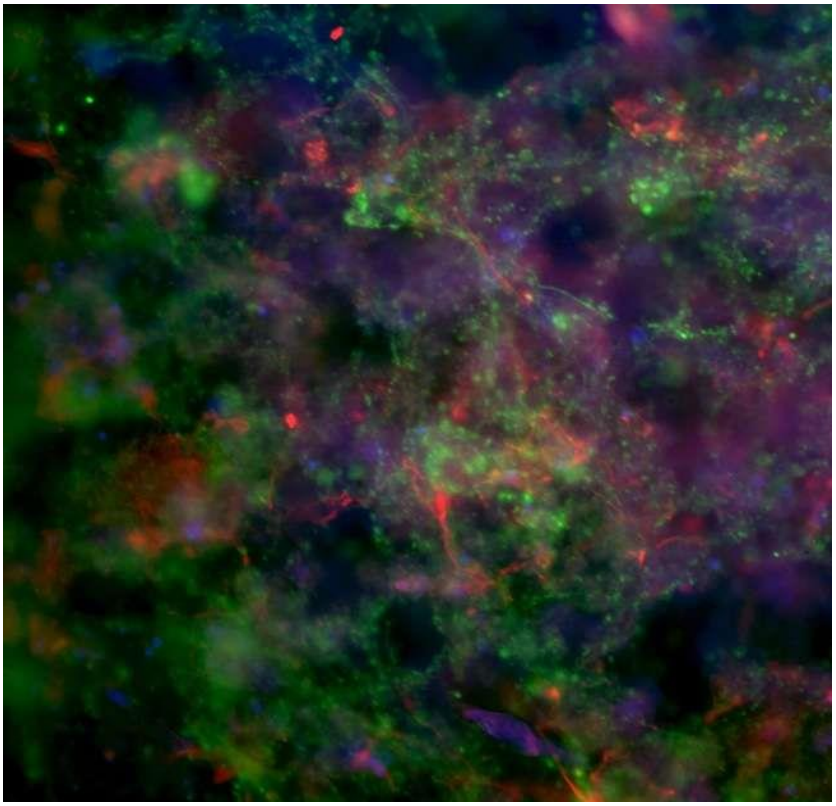

Figure 3.17 Example of immunofluorescence on 3D hydrogel culture.

Image acquired at 10x magnification and cultured at 103DIV with TubβIII (green), GFAP (red) and Dapi (blue).

Chapter 4

4. Results

- Twenty 2D samples were recorded whose spontaneous activity was captured up to DIV 41, of these, 9 showed exclusively sub-threshold activity and were excluded from the results.

- Two 3D samples were recorded whose spontaneous activity was captured up to DIV 109, of these, 1 showed exclusively sub-threshold activity and was excluded from the results.

- Eleven 3Dsu2D samples were recorded whose spontaneous activity was captured up to DIV 73, of these, 8 showed exclusively sub-threshold activity and were excluded from the results.

4.1 Qualitative analysis

Once the electrophysiological data has been recorded, we moved on to the manipulation of the same. The recordings were filtered (High Pass Butterworth 200Hz) and a spike detection algorithm (PTSD) was applied. The results produced by this algorithm highlight the spike events detected within the recorded signal. To verify if the PTSD algorithm was successful, but above all to obtain what is a first comparable data on the trend of the electrophysiological activity of the matrices, rasterplot graphs were produced.

The graphs show the electrophysiological activity recorded as a function of time of all 60 electrodes belonging to a matrix. The data obtained in the first 2 of the 10 minutes of recording are shown as they are in any case representative of the trend of the matrices.

4.1.1 2D samples

Since the 2D samples are very numerous (N=11), only the raster plots of a representative sample of the general evolutionary profile are shown.

From the Raster Plot graphs (Figure 4.1) one can immediately notice an evolution of the activity with the passage of time for the representative 2D culture.

This evolution takes the form of an overall increase in the spiking frequency and then takes the form of a progressive transition of the entire network to predominantly bursting activity, synchronized on all channels.

Furthermore, almost all the channels are active.

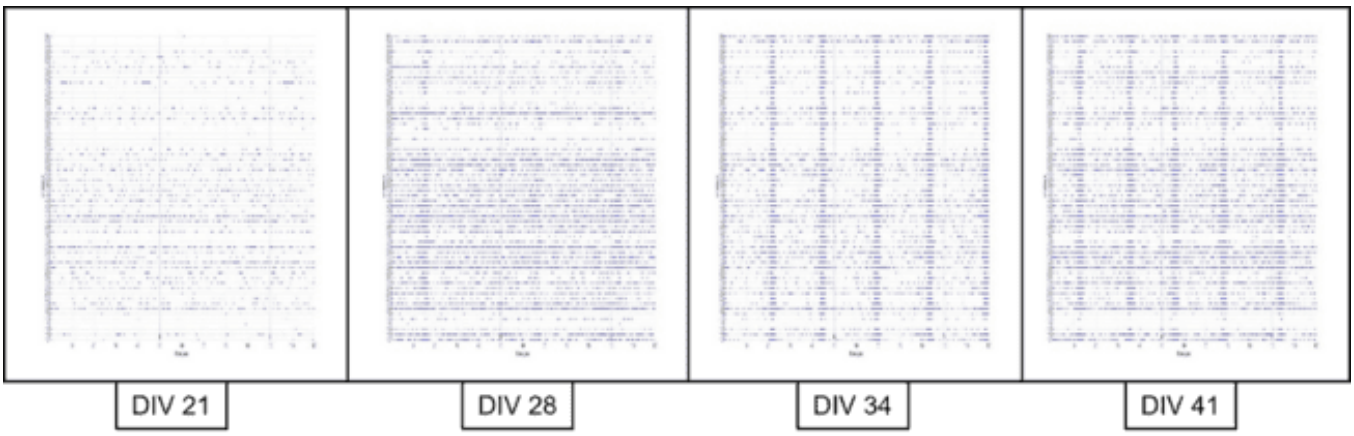

Figures 4.1 Raster Plot for representative 2D culture at DIV 21,28,34,41 respectively

4.1.2 3D sample

Given that the 3D samples were recorded for several days, in most of which no activity was seen, only the raster plots of the most salient recordings are shown, starting from the DIV in which a principle of activity was noticed, so to synthetically transmit the evolutionary profile of the sample.

From the Raster Plot graphs (Figure 4.2) it can immediately be seen that the 3D sample matures much more slowly than the 2D one. In fact, this does not show activity before DIV 46 when two channels begin to express a very slight spiking activity, this activity initially increases as the days go by, however most of the channels remain silent or in any case much less active than the remaining channels, which contrast show a moderate activity.

After this first increase, however, the activity lacks further evolution and remains substantially the same over time.

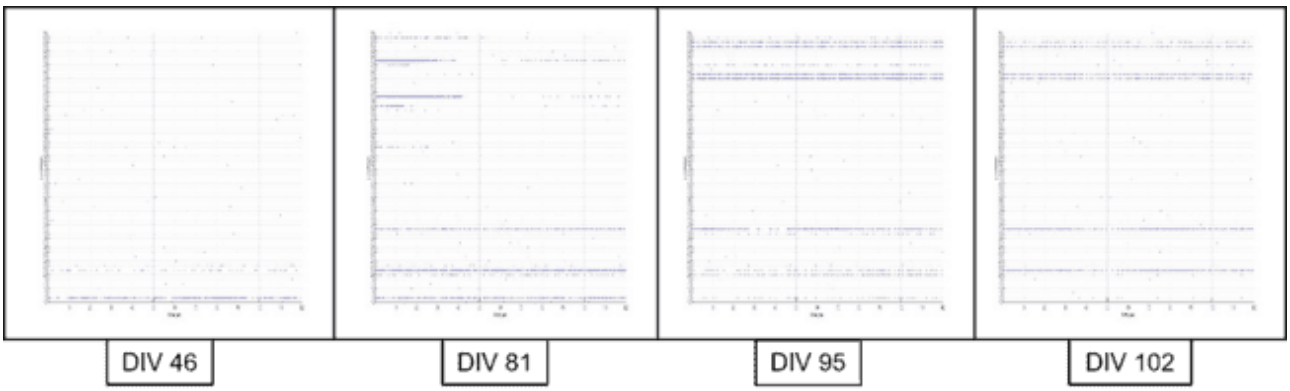

Figure 4.2 Raster Plot for representative 3D culture at DIV 46,81,95,102 respectively

4.1.3 3Don2D samples

Given that the 3Dsu2D samples were recorded for several days, most of which saw no activity, only the raster plots of the most salient recordings for each active sample are shown, to synthetically convey their evolutionary profile.

From the Raster Plot graphs (Figures 4.3, 4.4, 4.5) it can immediately be seen how, similarly to the 3D case, 3Don2D samples mature much more slowly than 2D. In fact, these do not show activity for most of their lives, and when they do, this activity is concentrated in a few channels and lacks evolution, remaining essentially the same over time, except for a tendency to switch from a mainly spiking activity to a mainly bursting one.

Furthermore, it can be noted how, despite the evolutionary profile being similar between the 3 samples, these develop on DIV which are considerably different from one sample to another; this, in conjunction with the low number of data points, did not allow to perform an average between samples as in the 2D case.

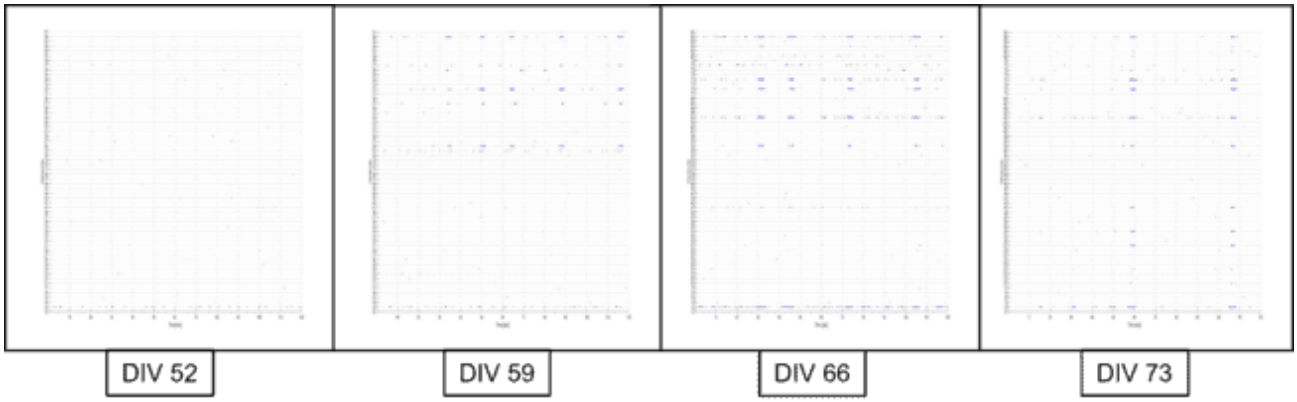

Figure 4.3 Raster Plot for 3Don2D A culture respectively at DIV 46,53,60,66

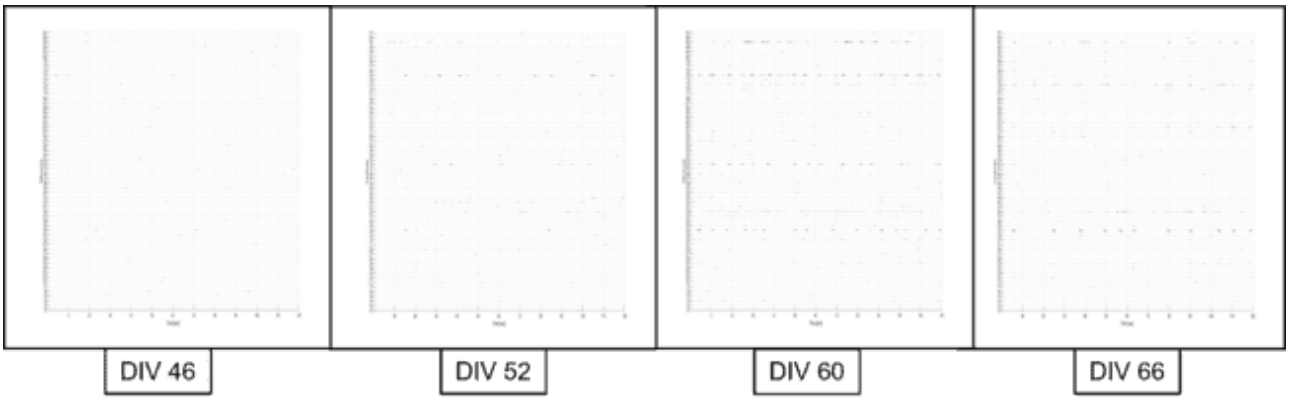

Figure 4.4 Raster Plot for 3Don2D B culture respectively at DIV 46,52,60,66

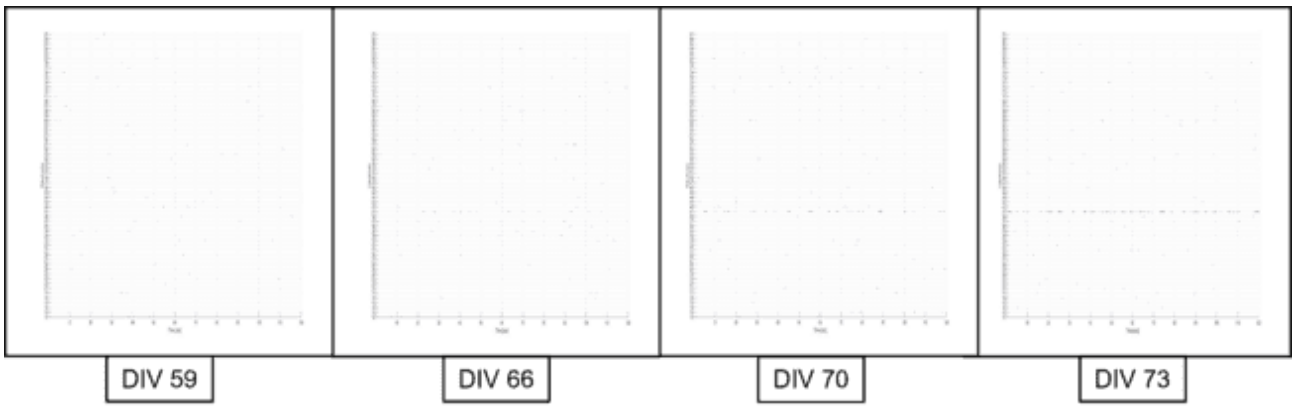

Figure 4.5 Raster Plot for 3Don2D C culture respectively at DIV 59,66,70,73

4.2 Quantitative Analysis

A quantitative analysis of the data was then carried out, evaluating the main parameters that can be extrapolated from the network which describe its dynamics:

- **Mean firing rate (spikes/sec)**
- **Burst Index (0 to 1)**
- **Mean burst rate (bursts/min)**
- **Mean burst duration (sec)**
- **Random spike rate (% of spikes out of bursts)**

With the aim of having a more significant understanding of the trend and of the functional modifications of the samples, the analysis was performed on the total number of channels belonging to each category in each recording time point. The data listed below therefore show the measurements of the average obtained day by day from the values of all the channels for each analysis group; in the case of the 2D models, the average of the channels of a single representative sample are represented first of all and subsequently the averages of the averages of all samples; in the case of 3D and 3D on 2D models only the averages on the channels of single representative matrices are represented.

An ANOVA statistical analysis was also performed for the 2D dataset, in particular the results of Bonferroni's Test ($p<0.05$) are integrated in the graphs.

Plots were produced using OriginLab software, statistical tests were performed using MATLAB and OriginLab, and measurements were expressed as mean ± standard error.

4.2.1 Representative 2D sample

Mean Firing Rate

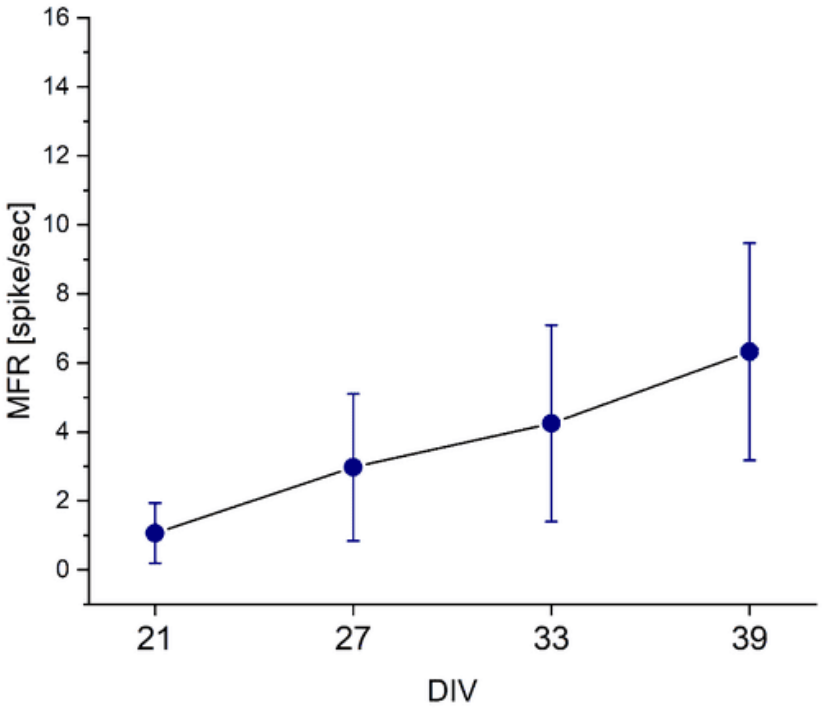

Figure 4.6 Representative 2D sample MFR trend

The graph (Figure 4.6) shows an almost linear growth of the MFR which coincides with the maturation of the sample and its increased activity.

Burst Index

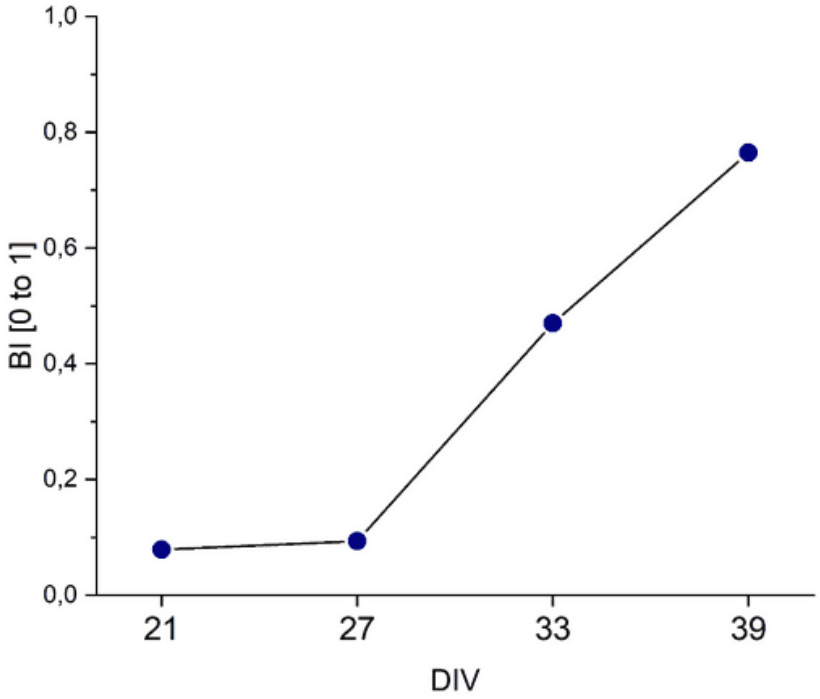

Figure 4.7 Trend BI representative 2D matrix

From the graph (Figure 4.7) the bursting activity is almost zero in the first two recording sessions, and then increases sharply in the last two, finally assuming an almost totally bursting behavior.

Mean Bursting Rate

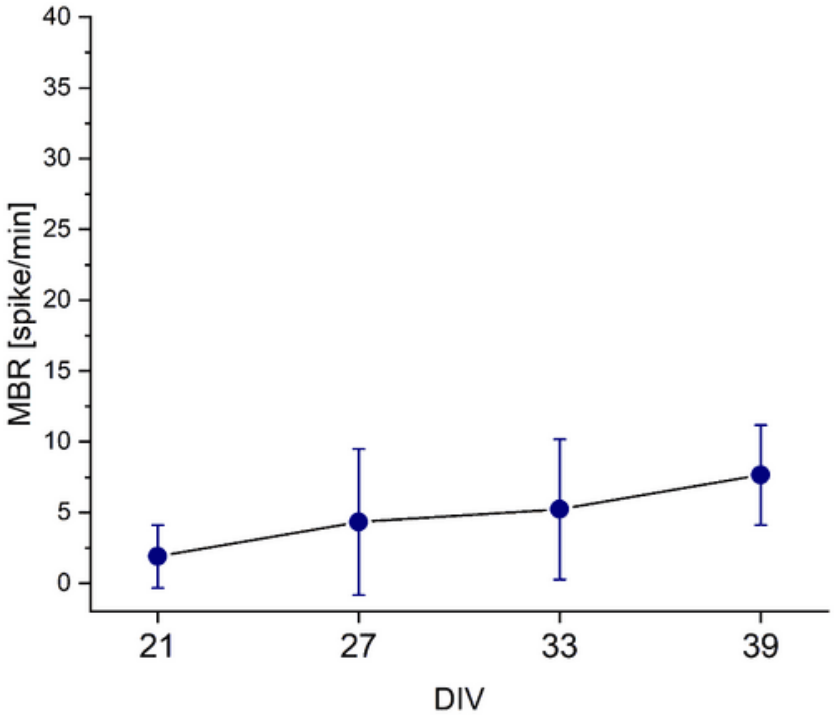

Figure 4.8 Representative 2D matrix MBR trend

From the graph (Figure 4.8) it can be seen that the MBR increases slightly as the days go by.

Mean bursting duration

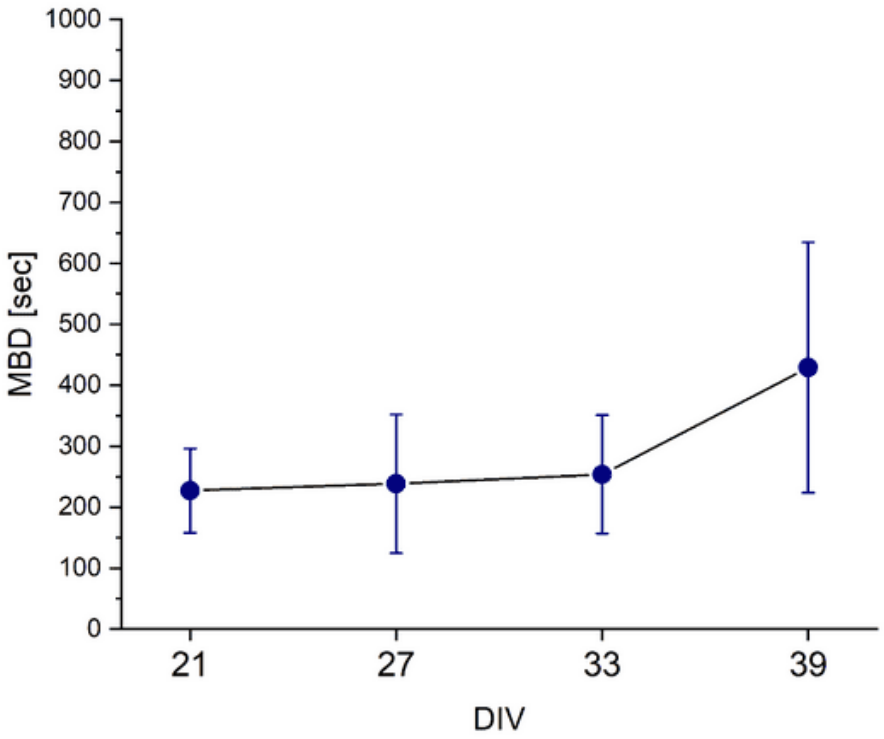

Figure 4.9 Representative 2D matrix MBD trend

From the graph (Figure 4.9) it can be seen that the MBD is almost constant for the first three sessions and then increases significantly in the last one.

Random Spikes

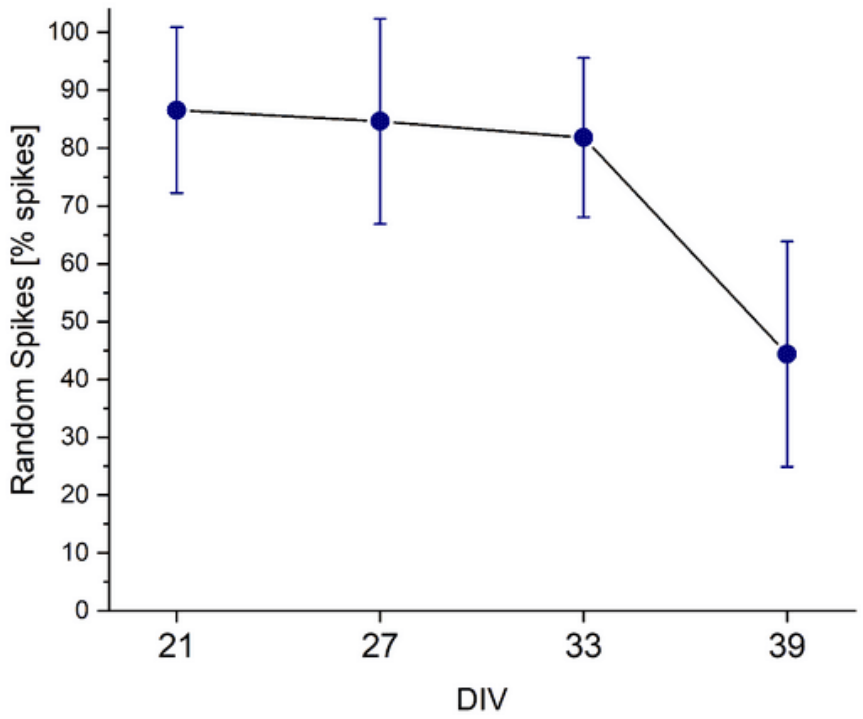

Figure 4.10 Random Spikes representative 2D matrix trend

From the graph (Figure 4.10) it can be seen that the number of random spikes outside the bursts decreases slightly for the first three sessions and then decreases significantly in the last one, indicating a predominantly bursting behavior.

Comments

Over time you may notice a:

- Considerable increase in firing rate
- Transition to a predominantly bursting activity (Burstiness Index tending towards 1 and decreasing Random Spike percentage)
- Results consistent with the literature

4.2.2 Analysis of the 2D dataset

Mean Firing Rate

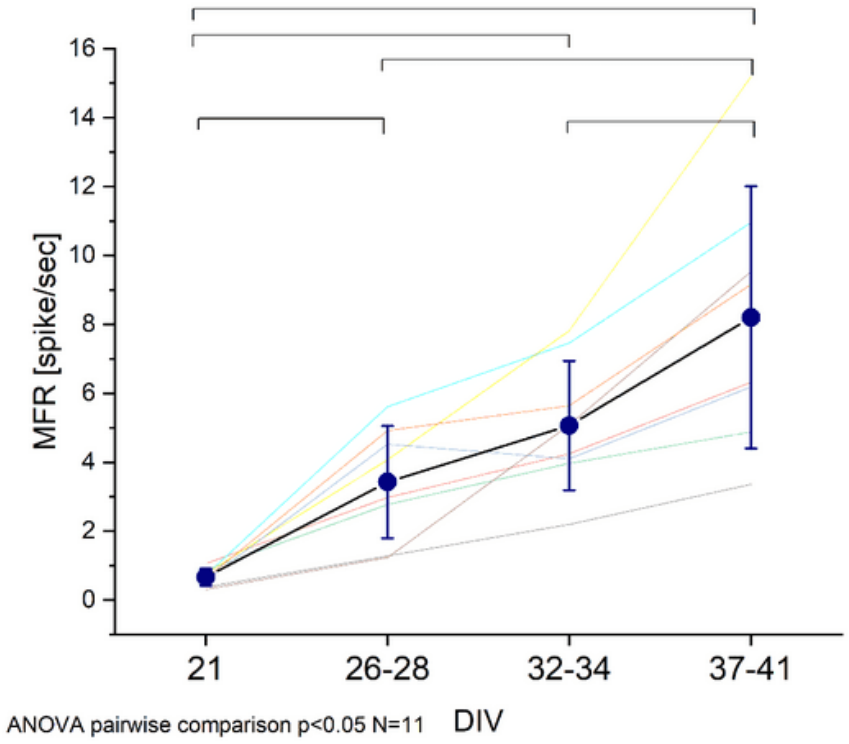

Figure 4.11 2D dataset MFR trend (average of samples in bold)

The graph (Figure 4.11) shows an almost linear growth of the MFR which coincides with the maturation of the samples and the increase in their activity.

Burst Index

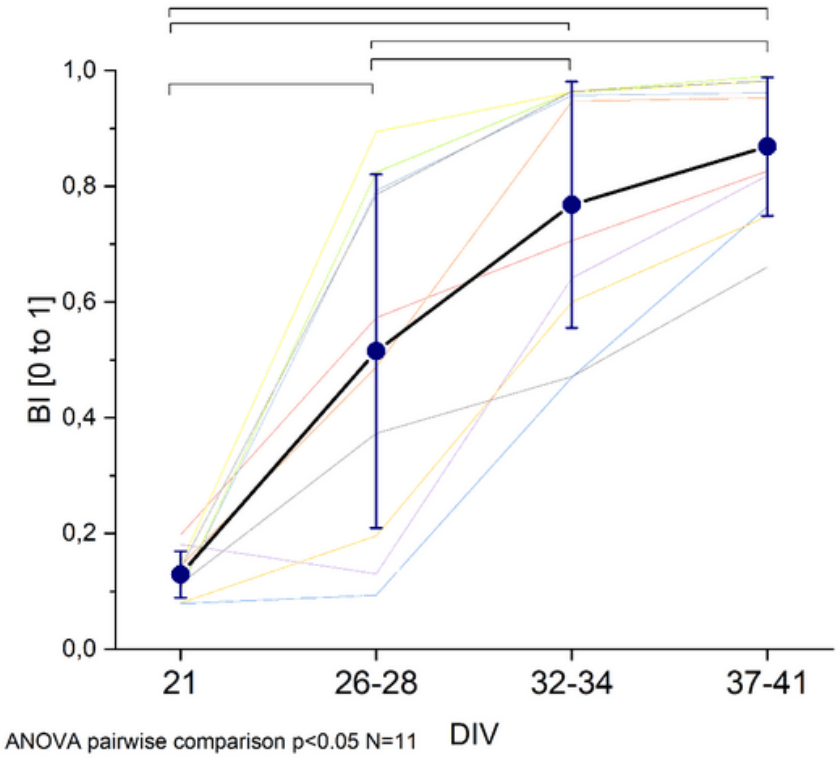

Figure 4.12 2D dataset BI trend (average of samples in bold)

From the graph (Figure 4.12) it can be seen that the bursting activity increases linearly with the maturation of the samples, finally assuming an almost totally bursting behavior.

Mean Bursting Rate

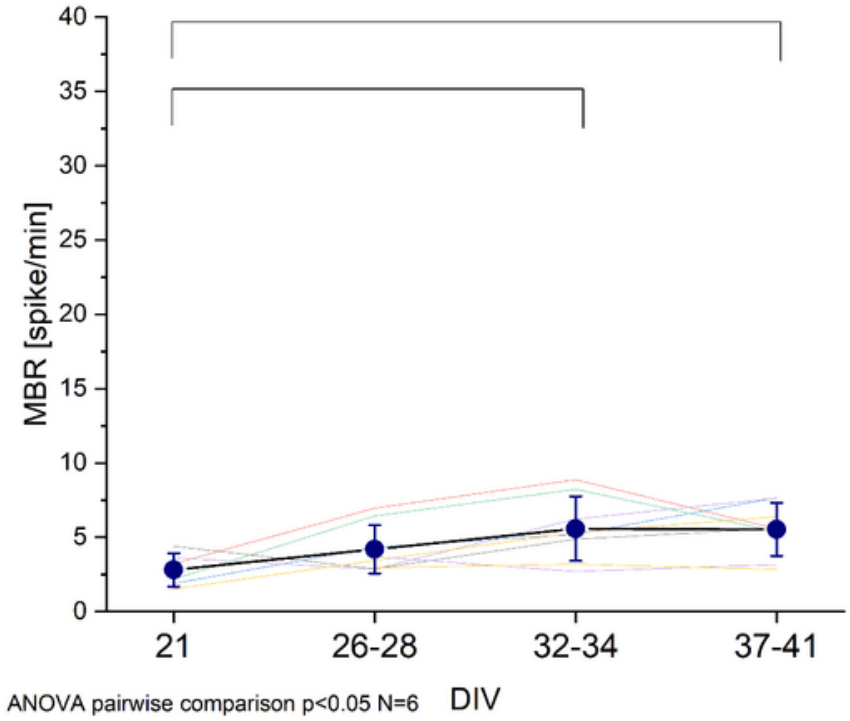

Figure 4.13 2D dataset MBR trend (average of samples in bold)

From the graph (Figure 4.13) it can be seen that the MBR increases slightly as the days go by but there is no significant evolution.

Mean bursting duration

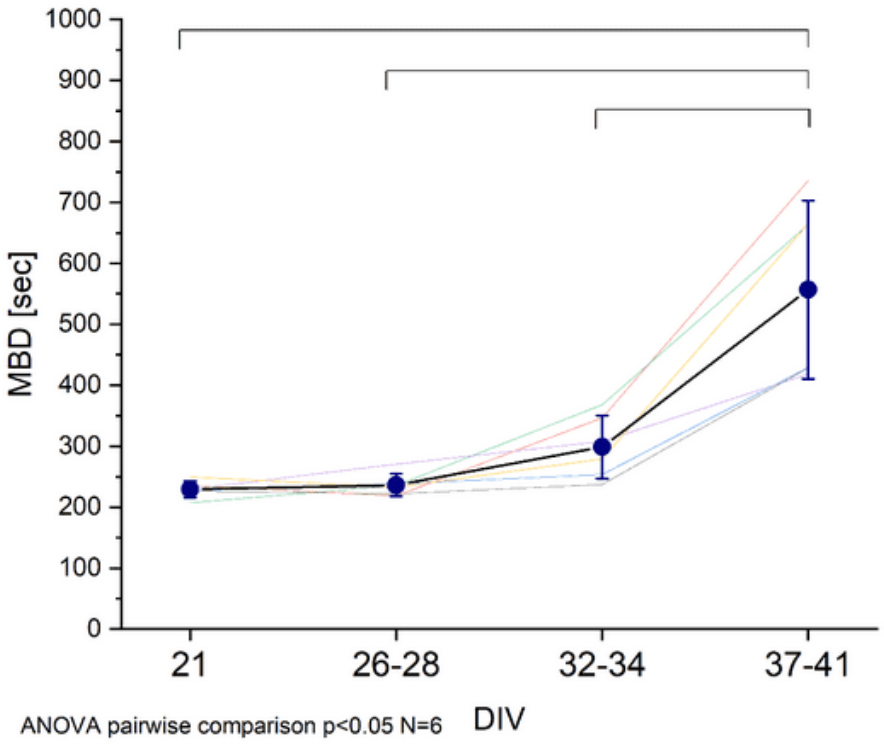

Figure 4.14 2D dataset MBD trend (average of samples in bold)

From the graph (Figure 4.14) it can be seen that the MBD is almost constant for the first three sessions and then increases significantly in the last one.

Random Spikes

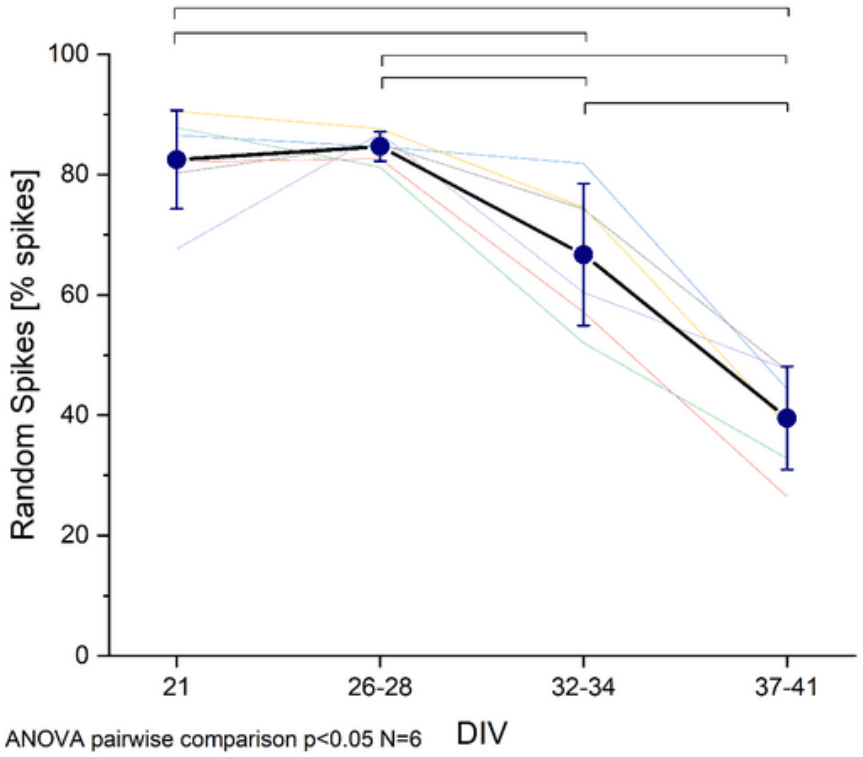

Figure 4.15 2D dataset Random Spikes trend (average of samples in bold)

From the graph (Figure 4.15) it can be seen that the number of random spikes outside the bursts is almost constant for the first two sessions and then decreases significantly in the last two, indicating a predominantly bursting behavior.

Comments

The recordings stopped at DIV 41 because the matrices were needed for other experiments, not for limitations of the 2D technology.

Over time you may notice a:

- Considerable increase in firing rate
- Transition to a predominantly bursting activity (Burstiness Index tending towards 1 and decreasing Random Spike percentage)
- Initial slight growth of the MBR to then settle at 5.5
- MBD almost unchanged initially and then doubled in the latest entry
- Results consistent with the literature

4.2.3 3D sample

Mean Firing Rate

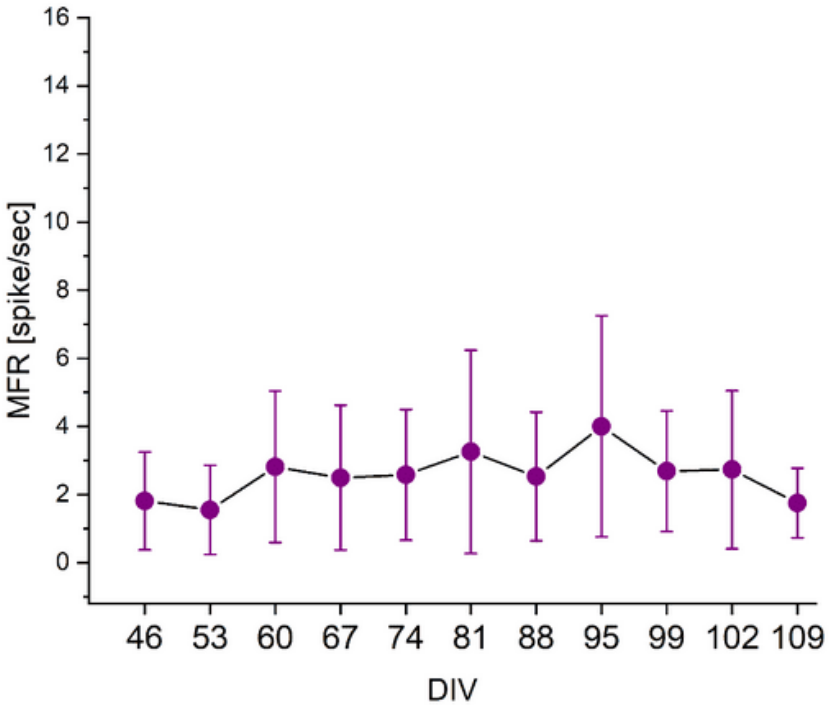

Figure 4.16 3D sample MFR trend

From the graph (Figure 4.16) you can see a slight overall growth of the MFR, unlike the 2D samples however this growth is very limited and overall there is no significant evolution of the activity as the days go by.

Burst Index

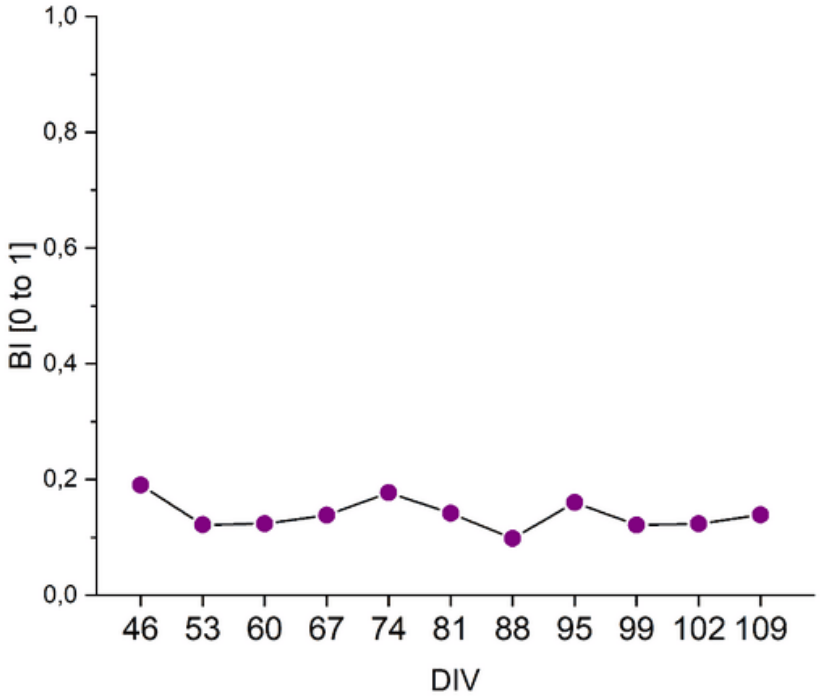

Figure 4.17 3D sample BI trend

From the graph (Figure 4.17) it can be seen that the bursting activity, unlike the 2D samples, remains overall around the same value even with the maturation of the sample.

Mean Bursting Rate

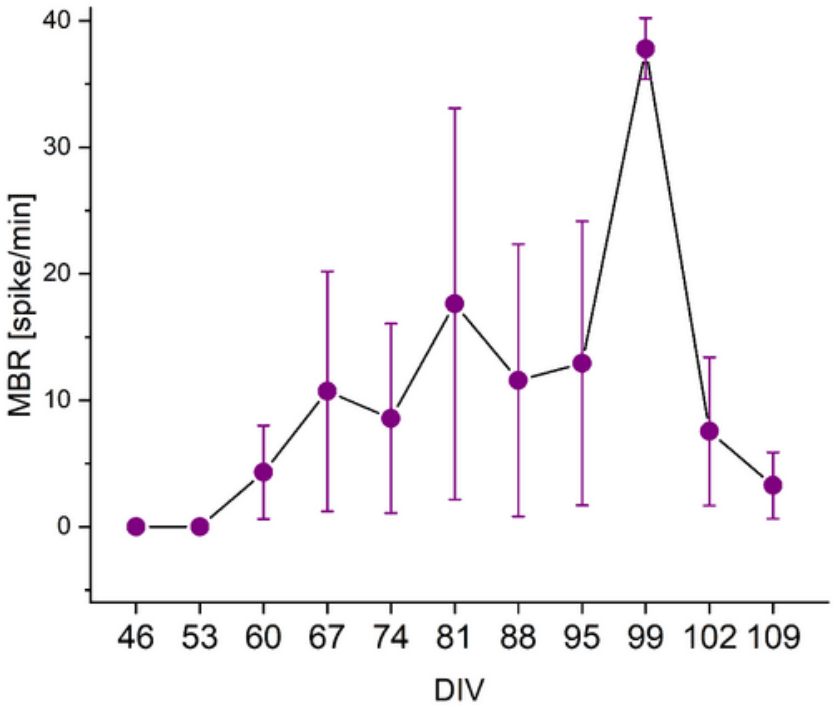

Figure 4.18 3D sample MBR trend

From the graph (Figure 4.18) it can be seen that the MBR, unlike 2D samples, is not very stable and grows at very high levels, however the variance is high, this is due to the fact that some channels are much more active than others.

Mean bursting duration

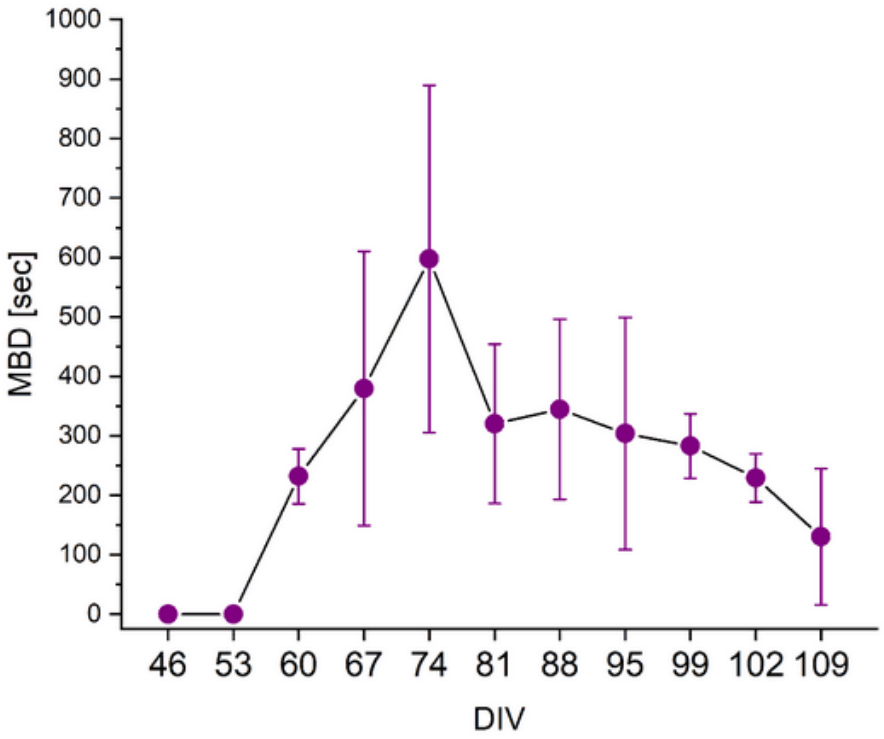

Figure 4.19 3D sample MBD trend

From the graph (Figure 4.19) it can be seen that the MBD for the first three sessions grows but from DIV81 it first drops drastically and then decreases more slowly, however the variance is high, this is due to the fact that some channels are much more active than others .

Random Spikes

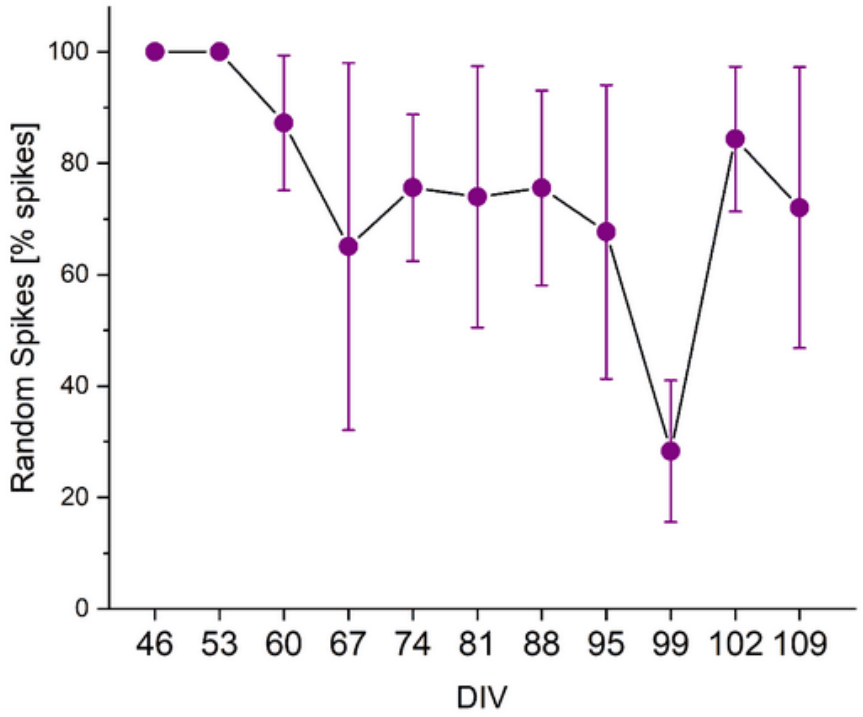

Figure 4.20 3D sample Random Spikes trend

From the graph (Figure 4.20) it can be seen that the number of random spikes outside the bursts fluctuates around 80% without significantly decreasing in sample maturation, excluding the DIV99 in which a drop of random spikes to around 30% is noted. which already at DIV102 go back to 85%.

Comments

- Channel average
- Sub-threshold activity up to DIV 46
- MFR increases slightly but remains around the same value therefore lack of evolution,
- High variance given by the fact that some channels are particularly active while others are not very active,
- Bursting frequent but limited to a large minority of channels
- Lower intensity than 2D,
- Registered for 109 DIV.

4.2.4 3Don2D A sample

Mean Firing Rate

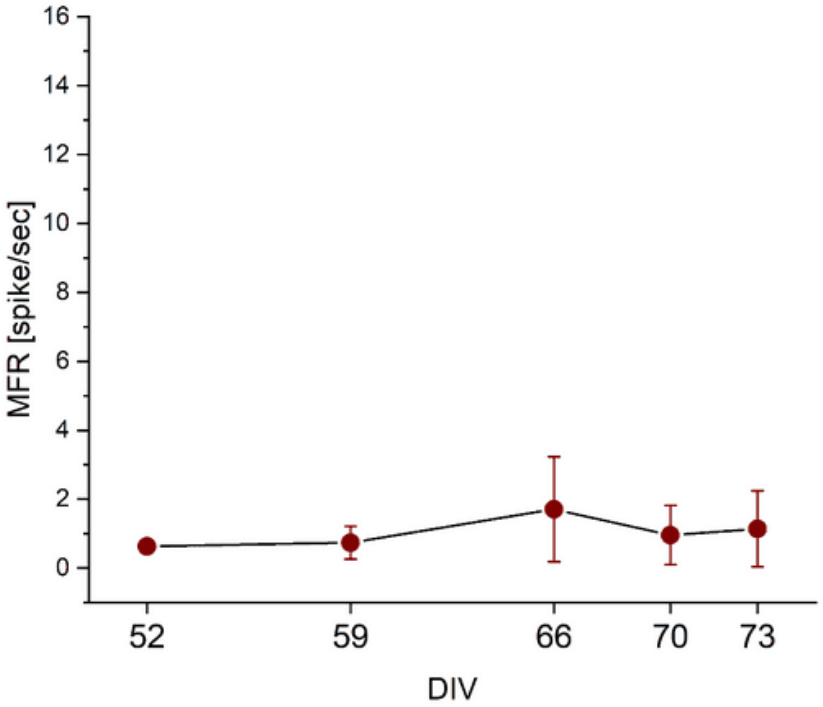

Figure 4.21 3Don2D A sample MFR trend

From the graph (Figure 4.21) you can see a very slight overall growth of the MFR but overall there is no significant evolution of the activity as the days go by.

Burst Index

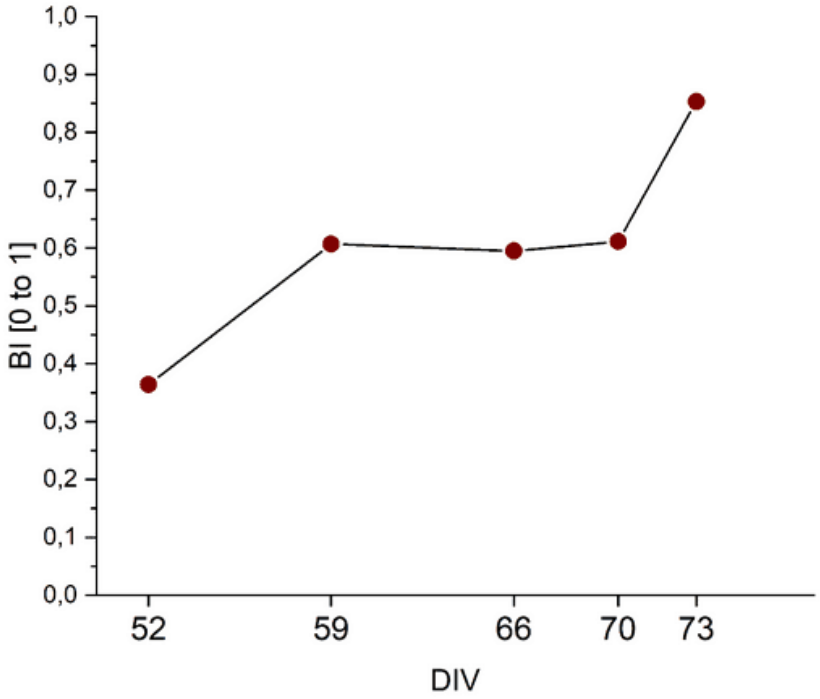

Figure 4.22 3Don2D A sample BI trend

From the graph (Figure 4.22) it can be seen that the bursting activity is lower but still appreciable, in the first two recording sessions, to then increase and remain stable on a BI of about 0.6 from DIV59 to DIV70, finally assuming an almost totally bursting at DIV73.

Mean Bursting Rate

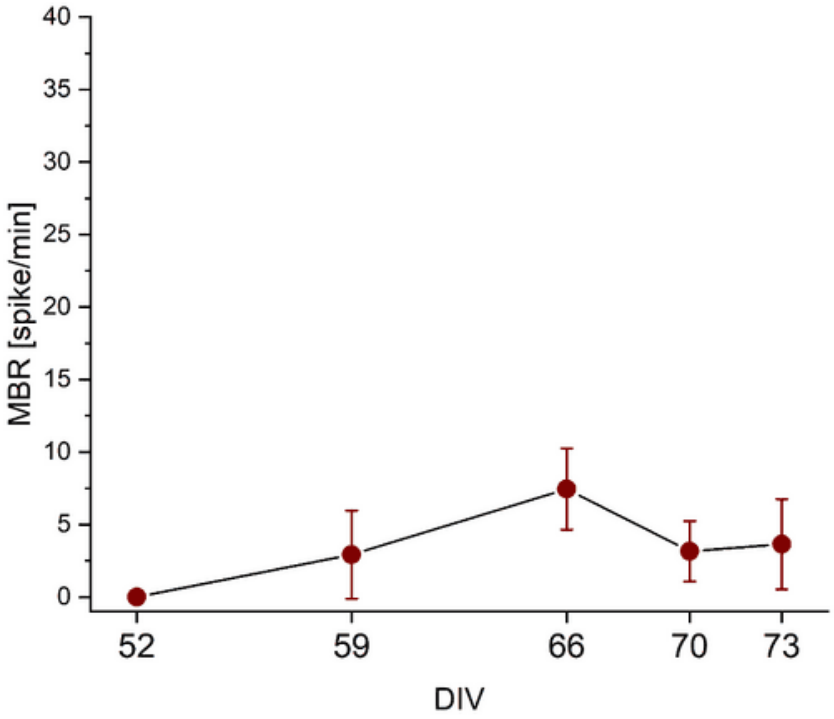

Figure 4.23 3Don2D A sample MBR trend

From the graph (Figure 4.23) you can see a slight overall growth of the MBR but overall there is no significant evolution of the activity as the days go by.

Mean bursting duration

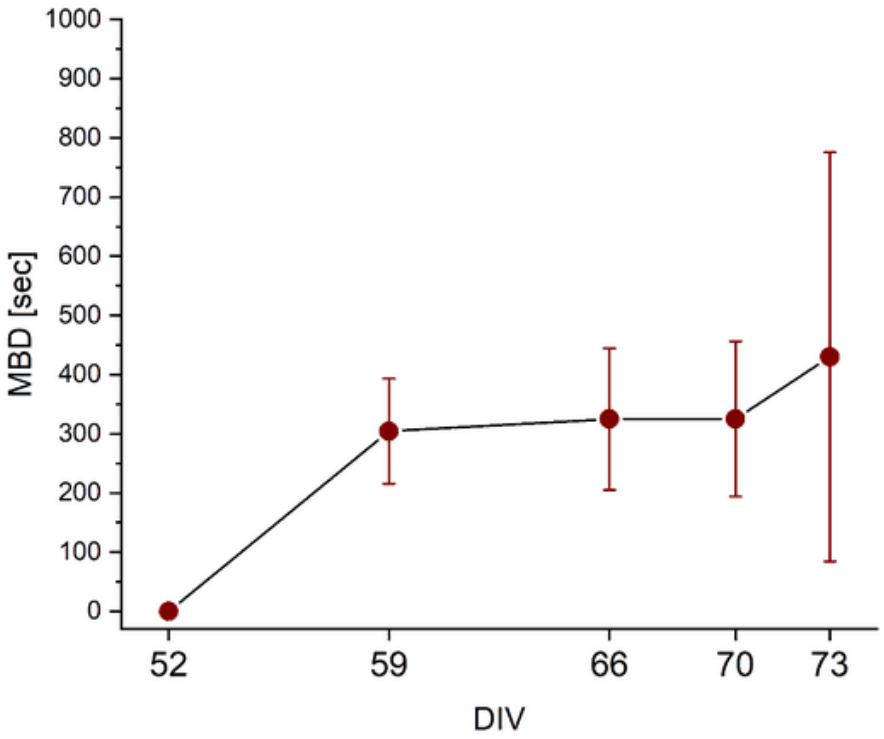

Figure 4.24 3Don2D A sample MBD trend

From the graph (Figure 4.24) we can see a slight overall growth of the MBD but overall there is no significant evolution of the activity as the days go by excluding the one between the first and second recording.

Random Spikes

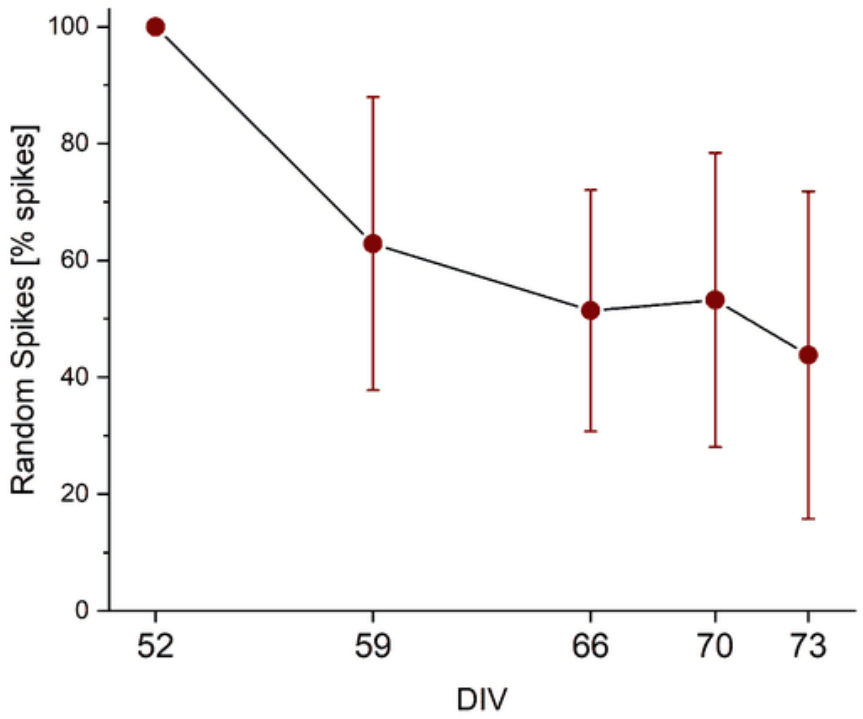

Figure 4.25 3Don2D A sample Random Spikes trend

From the graph (Figure 4.25) it can be seen that the number of random spikes outside the bursts is decreasing with the maturation of the sample, indicating a transition to a predominantly bursting dynamic.

Comments

- Channel average
- Below-threshold activity up to DIV 52,
- High variance for burst measurements given by the fact that some channels are particularly active while others are not very active,
- Lower intensity than 2D,
- Registered for 73 DIV,
- Over the time:
- MFR increases slightly but remains around the same value therefore lack of evolution
- Transition to an almost totally bursting activity (BI tending towards 1)

4.2.5 3Don2D B sample

Mean Firing Rate

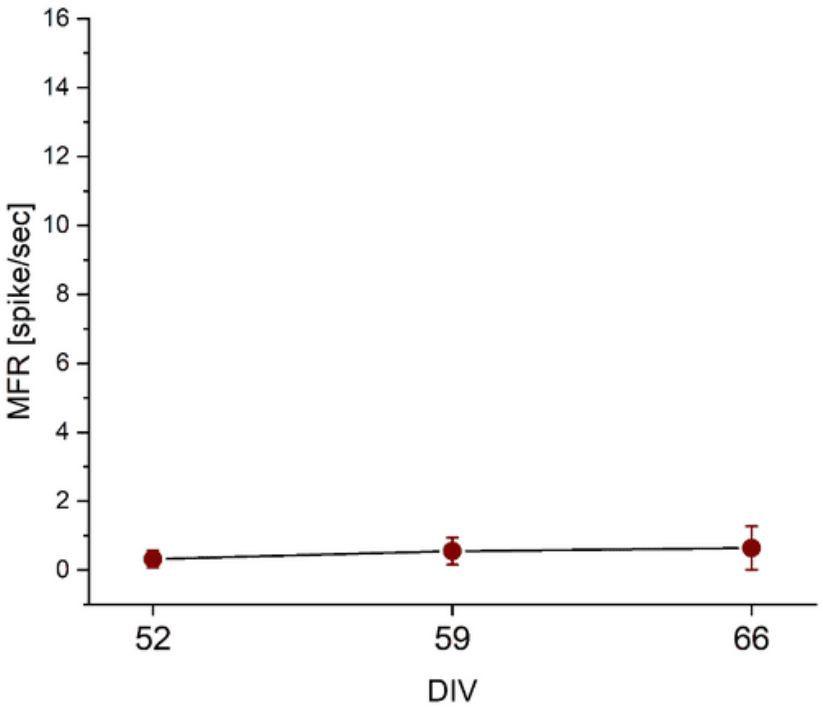

Figure 4.26 3Don2D B sample MFR trend

From the graph (Figure 4.26) you can see a very slight overall growth of the MFR but overall there is no significant evolution of the activity as the days go by.

Burst Index

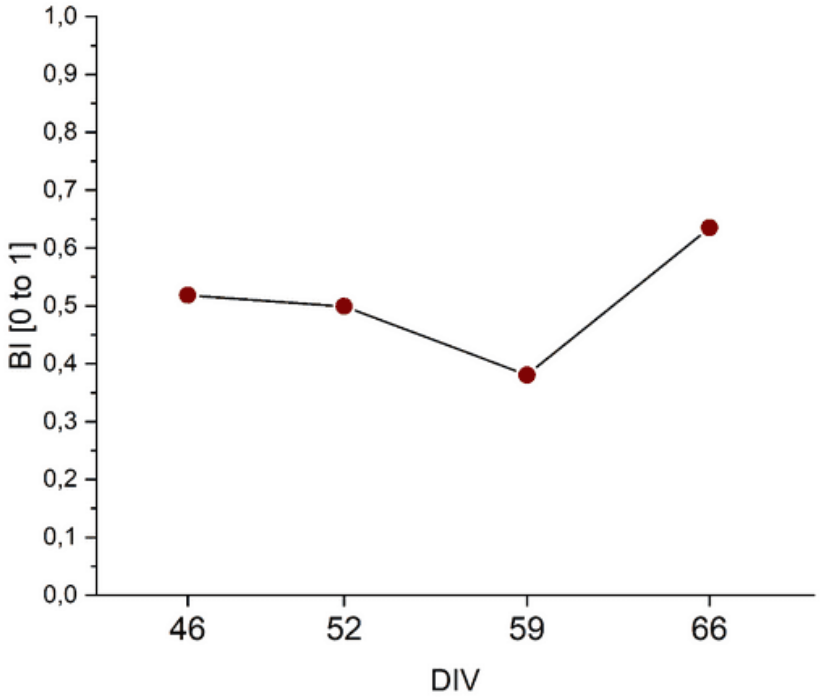

Figure 4.27 3Don2D B sample BI trend

From the graph (Figure 4.27) it can be seen that the bursting activity, unlike the 2D samples, is not very stable but increases slightly.

Mean Bursting Rate

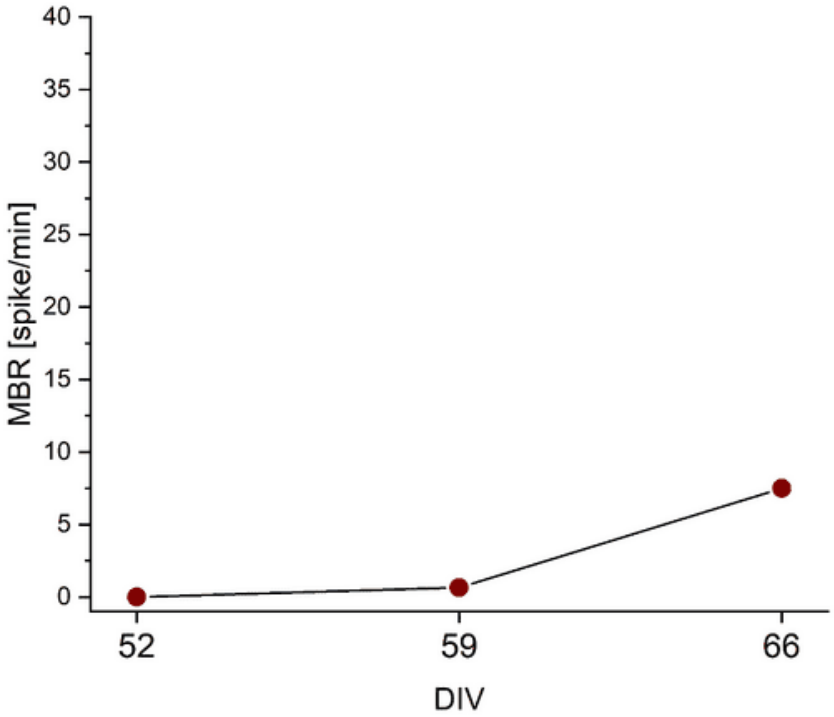

Figure 4.28 3Don2D B sample MBR trend

From the graph (Figure 4.28) it can be seen that the MBR increases significantly between DIV59 and DIV66.

Mean bursting duration

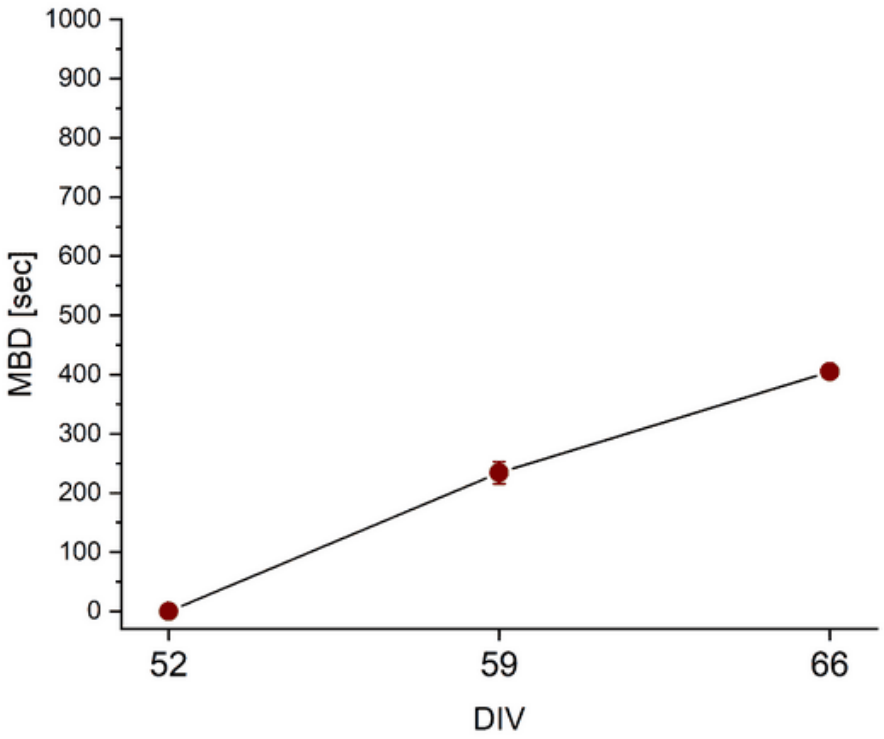

Figure 4.29 3Don 2D B sample MBD trend

From the graph (Figure 4.29) it can be seen that the MBD increases significantly with each passing day.

Random Spikes

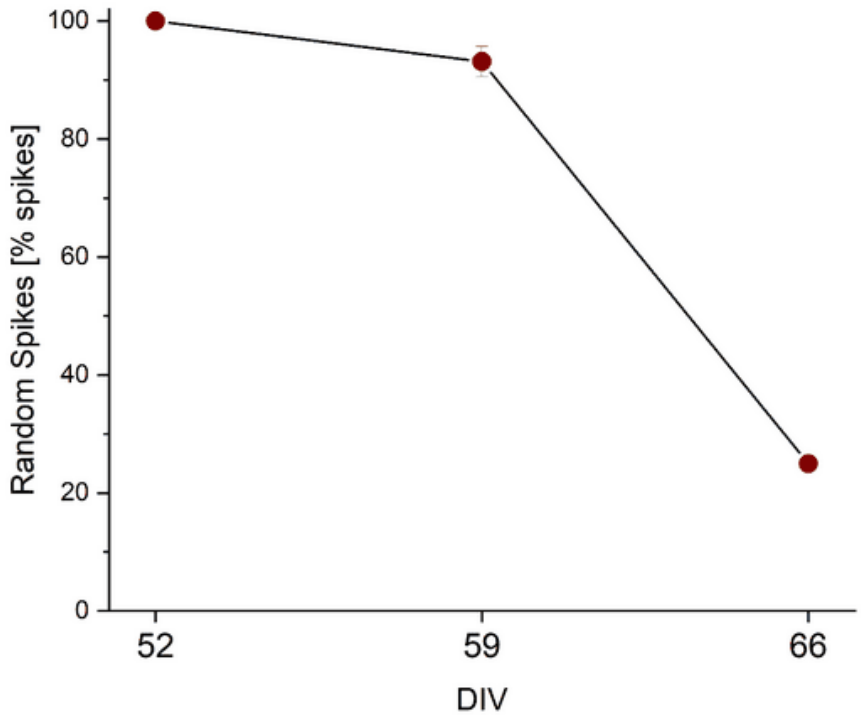

Figure 4.30 3Don2D B sample Random Spikes trend

From the graph (Figure 4.30) it can be seen that the number of random spikes outside the bursts is decreasing, indicating a trend towards bursting behavior.

Comments

- Channel average
- Below-threshold activity up to DIV 52,
- Lower intensity than 2D,
- Very few active channels but low variance as the other channels are essentially off so they have not returned to the average,
- Registered for 66 DIV,
- Over the time:
  - MFR remains around the same value therefore lack of evolution
  - Switching to a predominantly bursting activity

4.2.6 3Don2D C sample

Mean Firing Rate

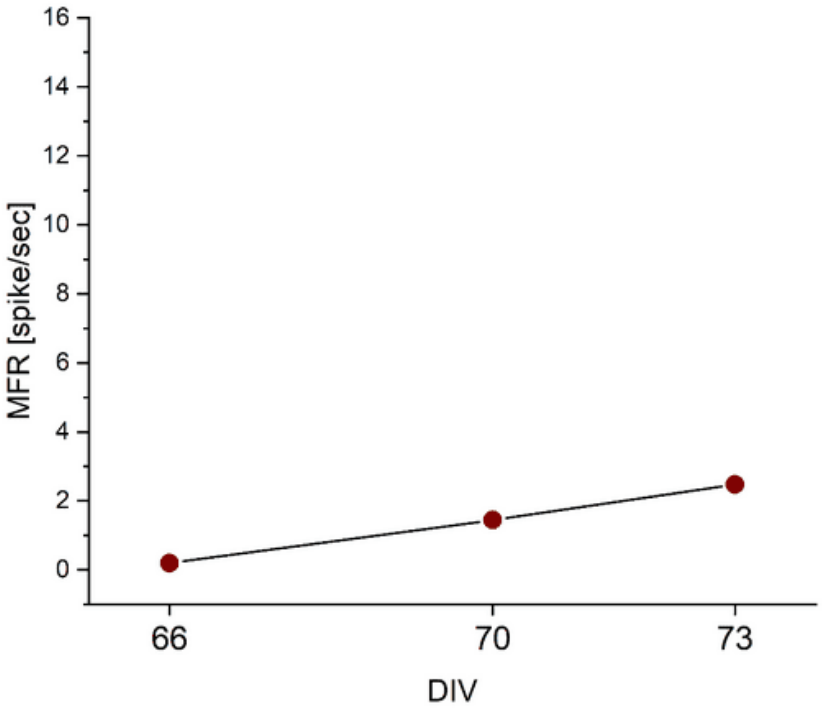

Figure 4.31 3Don2D C sample MFR trend

From the graph (Figure 4.31) you can see a slight overall growth of the MFR but overall there is no significant evolution of the activity as the days go by.

Burst Index

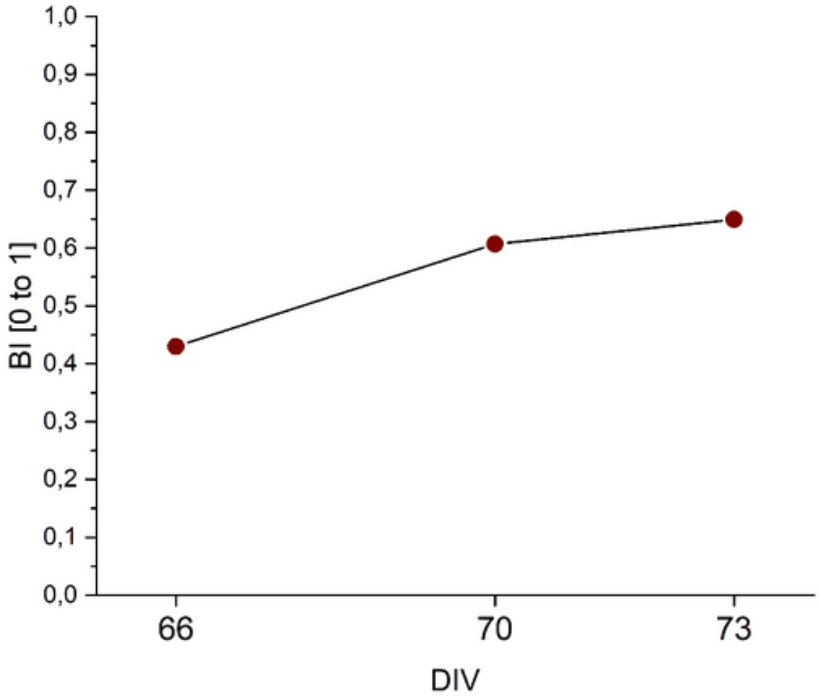

Figure 4.32 3Don2D C sample BI trend

From the graph (Figure 4.32) it can be seen that the bursting activity increases with the maturation of the samples.

Mean Bursting Rate

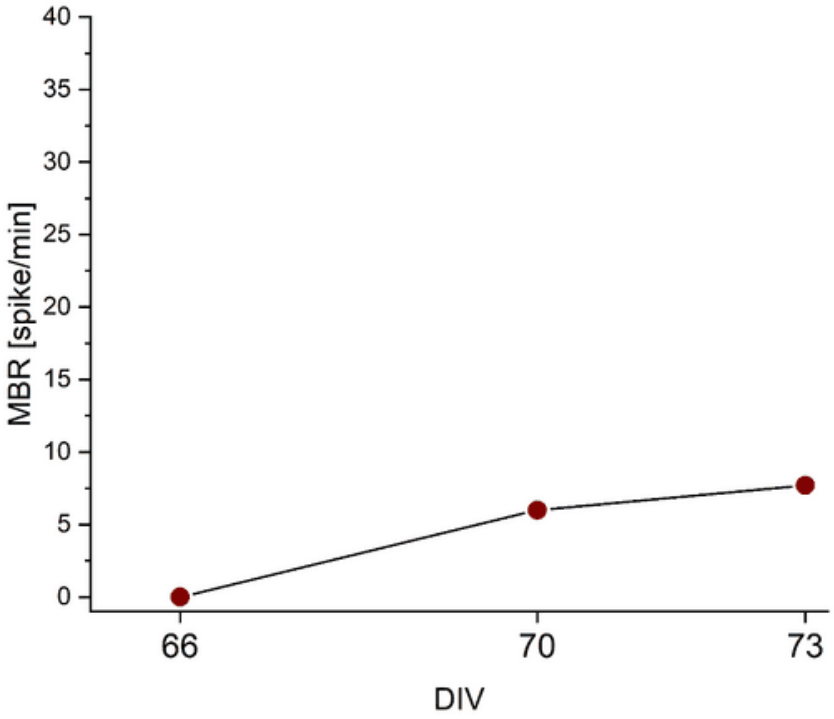

Figure 4.33 3Don2D C sample MBR trend

From the graph (Figure 4.33) it can be seen that the MBR increases significantly as the days go by.

Mean bursting duration

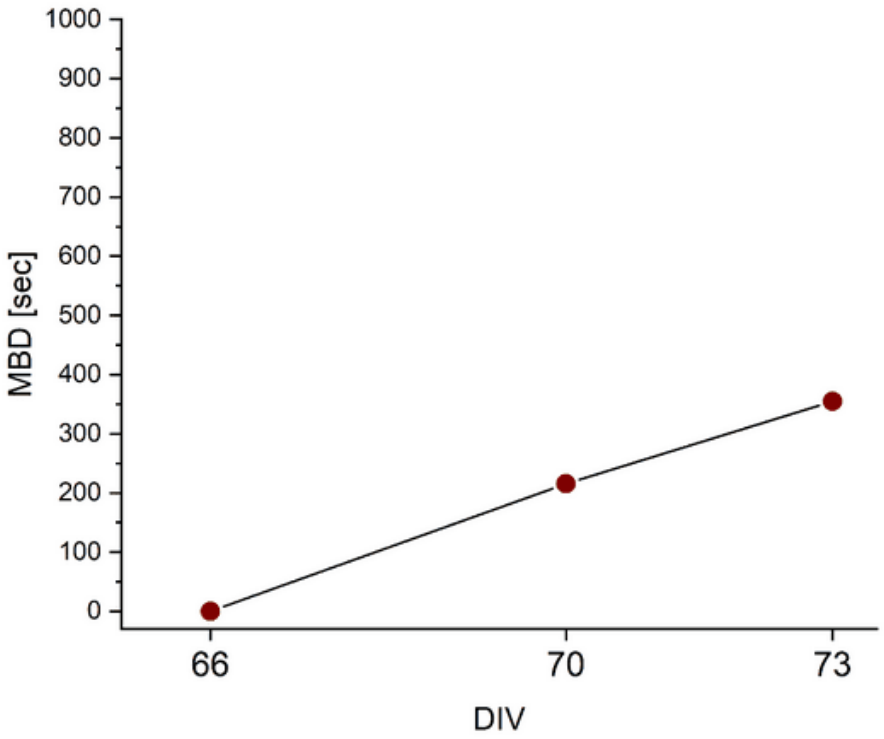

Figure 4.34 3Don2D C sample MBD trend

From the graph (Figure 4.34) it can be seen that the MBD increases significantly as the days go by.

Random Spikes

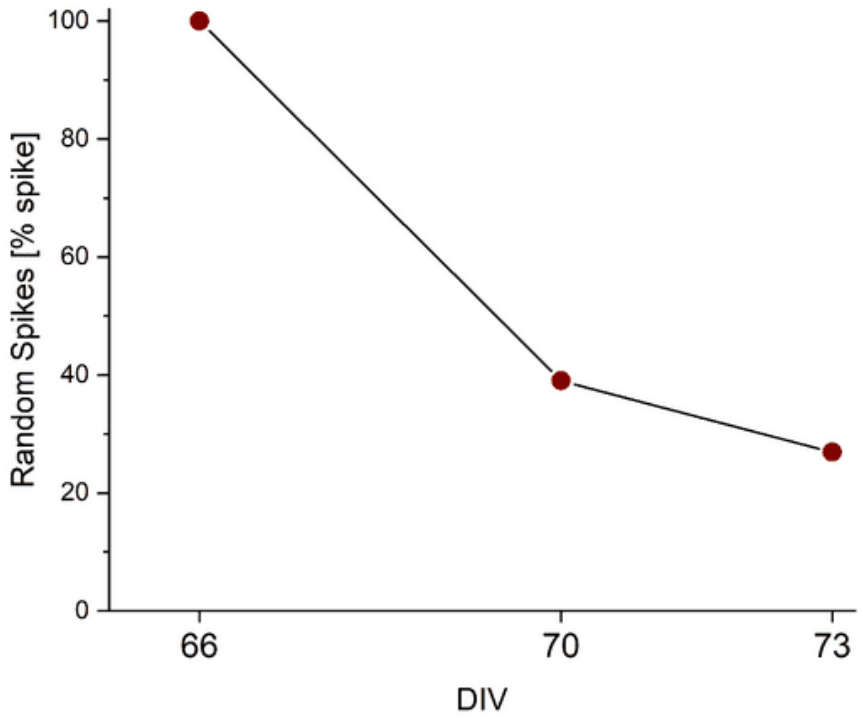

Figure 4.35 3Don2D C sample Random Spikes trend

From the graph (Figure 4.35) it can be seen that the number of random spikes outside the bursts is decreasing, indicating a trend towards bursting behavior.

Comments

- Channel average
- Sub-threshold activity up to DIV 66
- Very few active channels but low variance as the other channels are essentially off so they have not returned to the average,
- Lower intensity than 2D,
- Registered for 73 DIV,
- Over the time:
    - MFR increases slightly but overall lacks evolution
    - Switching to a predominantly bursting activity

4.3 Morphological Analysis

All the 3Dsu2D cultures under examination were fixed by PFA and each one was labeled using the immunofluorescence technique in order to evaluate their morphological characteristics.

The cellular components that have been highlighted are: the neuronal cytoskeleton by TubβIII marker, the glial fibrillar acid protein by GFAP and the nuclei by DAPI. All cultures were observed at three different magnifications: 10x, 20x, 50x.

From the images (Figure 4.36) it can be seen how neuronal cells tend to migrate towards the upper layers leaving the layer in contact with the electrodes uncovered by neurons, this may be a possible reason for the poor electrophysiological performance of 3D on 2D models, given that despite three-dimensional neuronal (labeled in TubβIII/green) and glial (labeled in GFAP/red) networks have formed, also visible in the images (Figure 4.6), the spontaneous functional activity is not recorded by the electrodes. In support of this, it can be noted that in the MEA3D models, whose needle electrodes manage to reach the uppermost layers, the spontaneous activity is considerably greater, albeit unstable.

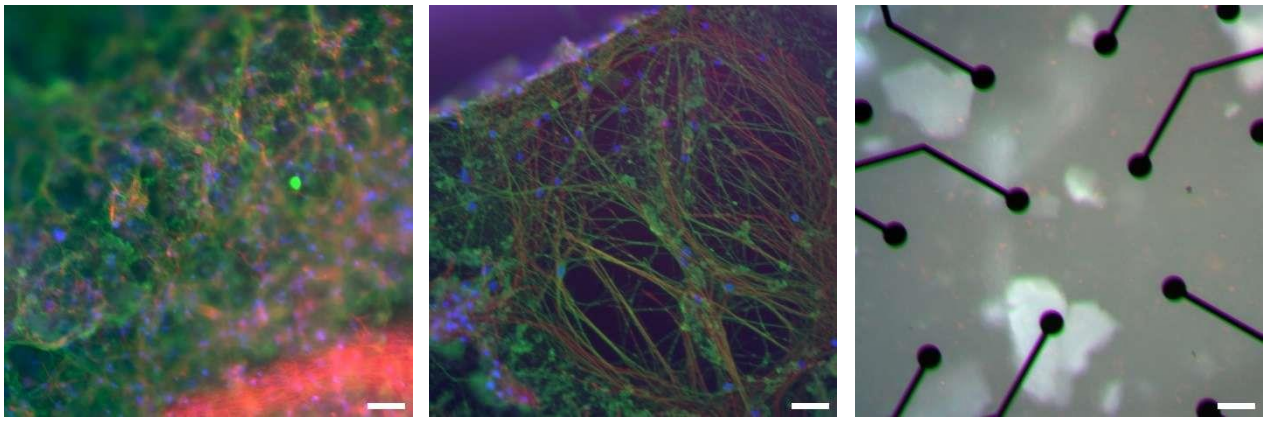

Figure 4.36 Images obtained by fluorescence optical microscopy. Images were acquired at 10x magnification and cultures labeled at DIV 73 with TubβIII (green), GFAP (red) and Dapi (blue). Scale bars 50 μm.

Conclusions

The aim of this thesis work was to construct and characterize *in vitro 2D and 3D networks* composed of neurons, differentiated from human induced pluripotent stem cells (h-iPSC), co-cultured with rat cortical astrocytes. In particular, different options of models and methodologies for the acquisition of the electrophysiological activity of the networks have been explored: 2D cultures on MEA2D, 3D cultures on MEA2D and 3D cultures on MEA3D.

The first part of this project involved the recording and analysis of the basal electrophysiological activity of the various types of cultures. The data acquisition took place by applying the registration protocol described in 2.2.3. The data from the registrations were processed and a qualitative analysis was conducted first followed by a quantitative one:

- For the qualitative analysis, rasterplot graphics were produced which showed a clear difference in the activity of the crops. In particular, 2D cultures show greater activity leading to faster maturation than 3D cultures and in particular 3D on 2D.
- In the quantitative analysis the previous results were confirmed. The parameters analyzed for 2D cultures show a progressive increase of the MFR starting as early as DIV 21, with a consequent transition to a predominantly bursting activity. For 3D cultures, the number of active channels is relatively low and no above-threshold activity is recorded before DIV 46; the MFR has values comparable to those of 2D cultures without, however, observing an increase over time; in contrast, both the frequency and duration of the bursts increase to much higher levels than in 2D cultures. For 3Don2D cultures many of the samples did not show above-threshold activity.

The second part of the work was dedicated to the morphological characterization of 3Dsu2D cultures to verify if their poor electrophysiological performance resulted from the lack of development of three-dimensional networks. Thanks to the immunofluorescence technique used, it emerged that:

- The scaffold supported the development and formation of a dense and highly morphologically connected three-dimensional network, both on the neuronal and glial cell side.
- The cells plated on the surface of the MEA migrated towards the upper layers of the hydrogel, preferring a "softer ″ support than glass and completely losing contact with the electrodes.

In conclusion, it can be stated that at the moment the methods of development and electrophysiological characterization of the 3D cultures represented in this thesis present critical issues: slower maturation, lower activity, high variance, few active channels; MEA3Ds appear more promising, mainly because of the much higher successful active culture percentage, but are more expensive and always have the limit of recording at the level of a single crop plane and not of various layers simultaneously.

However, it is necessary to distinguish which of these critical issues can be alleviated with different crop development protocols and which instead are intrinsic characteristics of 3D technology.

A possible way is to experiment with different concentrations of neuronal cells and, in the 3Dsu2D case, also different concentrations of adhesion factor and hydrogel, to ensure that the cells do not tend to migrate towards the upper layers, or to use or better develop a technology innovative that can be coupled with 3D cultures and that is able to effectively record the functional activity simultaneously from different heights of the culture, thus offering realistic and complete information of the models under study.

Appendix

Experiments with *In Vivo* probes

The possibility of using an acquisition system based on probes, typically used for *in vivo* recordings, capable of penetrating 3D cultures, was evaluated and explored.

Neuronexus A4x4-3mm-50-125-177 probes were used (Figure A.1), the complete acquisition setup (Figure A.2) also included a thermostat and a chamber for atmospheric control, similar to the cultures recorded on MEA.

The probe was inserted at different depths to probe the crops on several levels; however it was impossible to acquire any activity due to the very high noise, probably given by the non-optimal ground solution: a silver wire placed in contact with the culture medium.

A possible solution is to develop the cultures on MEA3D and exploit the MEA pins as ground in order to have a cleaner signal, however this introduces the risk of contact between the MEA electrodes and the Neuronexus probe, which given their fragility would result in probable damage to both.

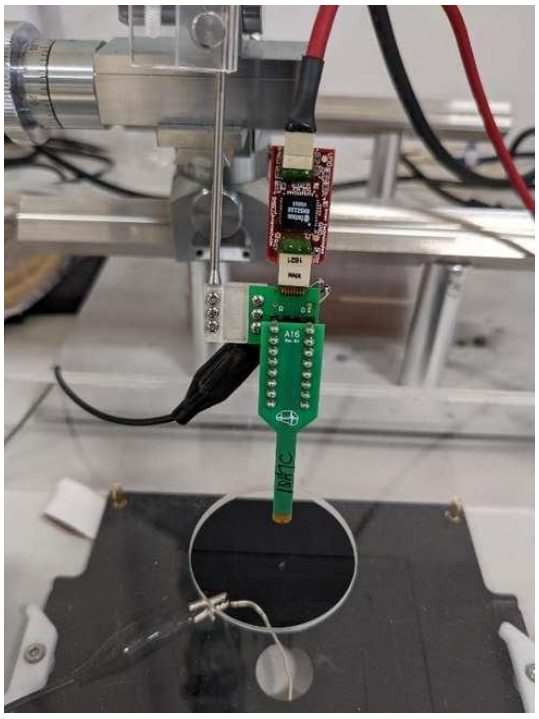

Figure A.1 Neuronexus probe A4x4-3mm-50-125-177

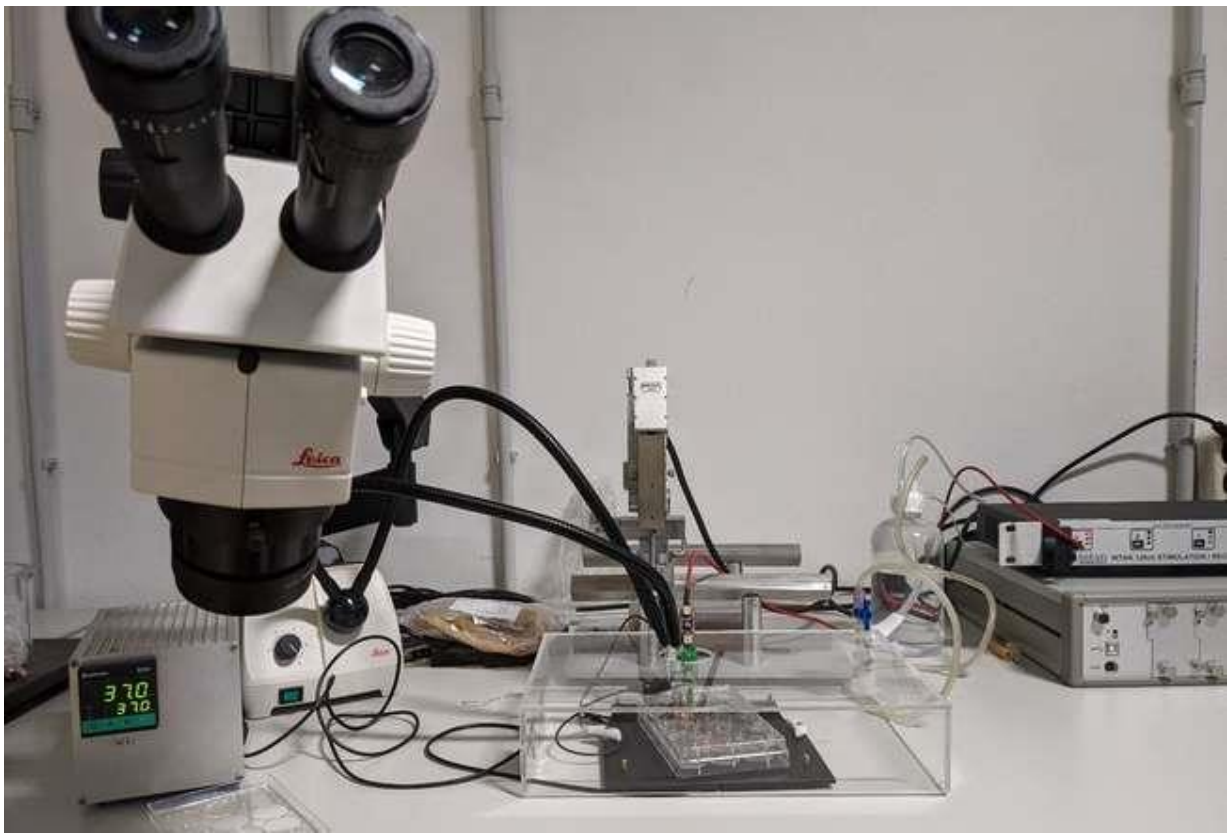

Figure A.2 Acquisition setup with complete Neuronexus probe

Bibliography

Amiri, M., Hosseinmardi, N., Bahrami, F., & Janahmadi, M. (2013). Astrocyte- neuron interaction as a mechanism responsible for generation of neural synchrony: A study based on modeling and experiments. *Journal of Computational Neuroscience*, *34*(3). https://doi.org/10.1007/s10827-012-0432-6

Araque, A., Parpura, V., Sanzgiri, R. P., & Haydon, P. G. (1999). Tripartite synapses: Glia, the unacknowledged partner. In *Trends in Neurosciences* (Vol. 22, Issue 5). https://doi.org/10.1016/S0166-2236(98)01349-6

Avoli, M., D'Antuono, M., Louvel, J., Köhling, R., Biagini, G., Pumain, R., D'Arcangelo, G., & Tancredi, V. (2002). Network and pharmacological mechanisms leading to epileptiform synchronization in the limbic system in vitro. In *Progress in Neurobiology* (Vol. 68, Issue 3). https://doi.org/10.1016/S0301-0082(02)00077-1

Bano, I., Arshad, M., Yasin, T., Ghauri, M. A., & Younus, M. (2017). Chitosan: A potential biopolymer for wound management. In *International Journal of Biological Macromolecules* (Vol. 102). https://doi.org/10.1016/j.ijbiomac.2017.04.047

Bazargani, N., & Attwell, D. (2016). Astrocyte calcium signaling: The third wave. In *Nature Neuroscience* (Vol. 19, Issue 2). https://doi.org/10.1038/nn.4201

Bear, M. F., Connors, B. W., & Paradiso, M. A. (2015). Neuroscience: Exploring the brain: Fourth edition. In *Neuroscience: Exploring the Brain: Fourth Edition*.

Bear, M. F., & Malenka, R. C. (1994). Synaptic plasticity: LTP and LTD. *Current Opinion in Neurobiology*, *4*(3). https://doi.org/10.1016/0959-4388(94)90101-5

Bliss, T. V. P., & Collingridge, G. L. (1993). A synaptic model of memory: Long-term potentiation in the hippocampus. In *Nature* (Vol. 361, Issue 6407). https://doi.org/10.1038/361031a0

Bliss, T. V. P., & Lømo, T. (1973). Long-lasting potentiation of synaptic transmission in the dentate area of the anaesthetized rabbit following stimulation of the perforant path. *The Journal of Physiology*, *232*(2). https://doi.org/10.1113/jphysiol.1973.sp010273

Bologna, L. L., Pasquale, V., Garofalo, M., Gandolfo, M., Baljon, P. L., Maccione, A., Martinoia, S., & Chiappalone, M. (2010). Investigating neuronal activity by SPYCODE multi-channel data analyzer. *Neural Networks*, *23*(6). https://doi.org/10.1016/j.neunet.2010.05.002

Boyle, J. (2005). Lehninger principles of biochemistry (4th ed.): Nelson, D., and Cox, M. *Biochemistry and Molecular Biology Education*, *33*(1). https://doi.org/10.1002/bmb.2005.494033010419

Buwalda, S. J., Boere, K. W. M., Dijkstra, P. J., Feijen, J., Vermonden, T., & Hennink, W. E. (2014). Hydrogels in a historical perspective: From simple networks to smart materials. In *Journal of Controlled Release* (Vol. 190). https://doi.org/10.1016/j.jconrel.2014.03.052

Buzsáki, G. (2006). Rhythms of the brain. *Oxford University Press.*

Buzsáki, G. (2002). Theta oscillations in the hippocampus. In *Neuron* (Vol. 33, Issue 3). https://doi.org/10.1016/S0896-6273(02)00586-X

Carpenter, M. K., Inokuma, M. S., Denham, J., Mujtaba, T., Chiu, C. P., & Rao, M. S. (2001). Enrichment of neurons and neural precursors from human embryonic stem cells. *Experimental Neurology*, *172*(2). https://doi.org/10.1006/exnr.2001.7832

Chaicharoenaudomrung, N., Kunhorm, P., & Noisa, P. (2019). Three-dimensional cell culture systems as an in vitro platform for cancer and stem cell modeling. In *World Journal of Stem Cells* (Vol. 11, Issue 12). https://doi.org/10.4252/wjsc.v11.i12.1065

Chiappalone, M., Bove, M., Vato, A., Tedesco, M., & Martinoia, S. (2006). Dissociated cortical networks show spontaneously correlated activity patterns during in vitro development. *Brain Research*, *1093*(1). https://doi.org/10.1016/j.brainres.2006.03.049

Cui, J., Xu, L., Bressler, S. L., Ding, M., & Liang, H. (2008). BSMART: A Matlab/C toolbox for analysis of multichannel neural time series. *Neural Networks*, *21*(8). https://doi.org/10.1016/j.neunet.2008.05.007

Day, J. J., & Sweatt, J. D. (2011). Epigenetic Mechanisms in Cognition. In *Neuron* (Vol. 70, Issue 5). https://doi.org/10.1016/j.neuron.2011.05.019

De Masi, A., Tonazzini, I., Masciullo, C., Mezzena, R., Chiellini, F., Puppi, D., & Cecchini, M. (2019). Chitosan films for regenerative medicine: fabrication methods and mechanical characterization of nanostructured chitosan films. In *Biophysical Reviews* (Vol. 11, Issue 5). https://doi.org/10.1007/s12551-019-00591-6

Di Lisa, D., Muzzi, L., Pepe, S., Dellacasa, E., Frega, M., Fassio, A., Martinoia, S., & Pastorino, L. (2022). On the way back from 3D to 2D: Chitosan promotes adhesion and development of neuronal networks onto culture supports. *Carbohydrate Polymers*, *297*. https://doi.org/10.1016/j.carbpol.2022.120049

Di Lisa, D., Tedesco, M., Dellacasa, E., Pesce, M., Catelani, T., Massobrio, P., Raiteri, R., Martinoia, S., & Pastorino, L. (2020). Chitosan biopolymer: Alternative adhesion factor and scaffold matrix for 2D and 3D neuronal cultures. *Biomedical Science and Engineering*, *3*(s3). https://doi.org/10.4081/bse.2019.107

Diekelmann, S., & Born, J. (2010). The memory function of sleep. In *Nature Reviews Neuroscience* (Vol. 11, Issue 2). https://doi.org/10.1038/nrn2762

Dudek, S. M., & Bear, M. F. (1992). Homosynaptic long-term depression in area CA1 of hippocampus and effects of N-methyl-D-aspartate receptor blockade. *Proceedings of the National Academy of Sciences of the United States of America*, *89*(10). https://doi.org/10.1073/pnas.89.10.4363

Egert, U., Knott, T., Schwarz, C., Nawrot, M., Brandt, A., Rotter, S., & Diesmann, M. (2002). MEA-Tools: An open source toolbox for the analysis of multi-electrode data with MATLAB. *Journal of Neuroscience Methods*, *117*(1). https://doi.org/10.1016/S0165-0270(02)00045-6

Engler, A. J., Sen, S., Sweeney, H. L., & Discher, D. E. (2006). Matrix Elasticity Directs Stem Cell Lineage Specification. *Cell*, *126*(4). https://doi.org/10.1016/j.cell.2006.06.044

Freeman, M. R. (2010). Specification and morphogenesis of astrocytes. In *Science* (Vol. 330, Issue 6005). https://doi.org/10.1126/science.1190928

Geckil, H., Xu, F., Zhang, X., Moon, S., & Demirci, U. (2010). Engineering hydrogels as extracellular matrix mimics. In *Nanomedicine* (Vol. 5, Issue 3). https://doi.org/10.2217/nnm.10.12

Georges, P. C., & Janmey, P. A. (2005). Cell type-specific response to growth on soft materials. In *Journal of Applied Physiology* (Vol. 98, Issue 4). https://doi.org/10.1152/japplphysiol.01121.2004

Gomi, H., Yokoyama, T., & Itohara, S. (2010). Role of GFAP in morphological retention and distribution of reactive astrocytes induced by scrapie encephalopathy in mice. *Brain Research*, *1312*. https://doi.org/10.1016/j.brainres.2009.11.025

Guan, X., Avci-Adali, M., Alarçin, E., Cheng, H., Kashaf, S. S., Li, Y., Chawla, A., Jang, H. L., & Khademhosseini, A. (2017). Development of hydrogels for regenerative engineering. In *Biotechnology Journal* (Vol. 12, Issue 5). https://doi.org/10.1002/biot.201600394

Hagg, T., Muir, D., Engvall, E., Varon, S., & Manthorpe, M. (1989). Laminin-like antigen in rat CNS neurons: Distribution and changes upon brain injury and nerve growth factor treatment. *Neuron*, *3*(6). https://doi.org/10.1016/0896-6273(89)90241-9

Harrison, R. G., Greenman, M. J., Mall, F. P., & Jackson, C. M. (1907). Observations of the living developing nerve fiber. *The Anatomical Record*, *1*(5). https://doi.org/10.1002/ar.1090010503

Hatten, M. E., Furie, M. B., & Rifkin, D. B. (1982). Binding of developing mouse cerebellar cells to fibronectin: A possible mechanism for the formation of the external granular layer. *Journal of Neuroscience*, *2*(9). https://doi.org/10.1523/jneurosci.02-09-01195.1982

Hirano, S. (1996). Chitin Biotechnology Applications. *Biotechnology Annual Review*, *2*(C). https://doi.org/10.1016/S1387-2656(08)70012-7

Hughes, S. W., Blethyn, K. L., Cope, D. W., & Crunelli, V. (2002). Properties and origin of spikelets in thalamocortical neurones in vitro. *Neuroscience*, *110*(3). https://doi.org/10.1016/S0306-4522(01)00577-2

Kamioka, H., Maeda, E., Jimbo, Y., Robinson, H. P. C., & Kawana, A. (1996). Spontaneous periodic synchronized bursting during formation of mature patterns of connections in cortical cultures. *Neuroscience Letters*, *206*(2–3). https://doi.org/10.1016/S0304-3940(96)12448-4

Kim, I. Y., Seo, S. J., Moon, H. S., Yoo, M. K., Park, I. Y., Kim, B. C., & Cho, C. S. (2008). Chitosan and its derivatives for tissue engineering applications. In *Biotechnology Advances* (Vol. 26, Issue 1). https://doi.org/10.1016/j.biotechadv.2007.07.009

Li, L., Lundkvist, A., Andersson, D., Wilhelmsson, U., Nagai, N., Pardo, A. C., Nodin, C., Ståhlberg, A., Aprico, K., Larsson, K., Yabe, T., Moons, L., Fotheringham, A., Davies, I., Carmeliet, P., Schwartz, J. P., Pekna, M., Kubista, M., Blomstrand, F., … Pekny, M. (2008). Protective role of reactive astrocytes in brain ischemia. *Journal of Cerebral Blood Flow and Metabolism*, *28*(3). https://doi.org/10.1038/sj.jcbfm.9600546

Maccione, A., Gandolfo, M., Massobrio, P., Novellino, A., Martinoia, S., & Chiappalone, M. (2009). A novel algorithm for precise identification of spikes in extracellularly recorded neuronal signals. *Journal of Neuroscience Methods*, *177*(1). https://doi.org/10.1016/j.jneumeth.2008.09.026

Malenka, R. C., & Bear, M. F. (2004). LTP and LTD: An embarrassment of riches. In *Neuron* (Vol. 44, Issue 1). https://doi.org/10.1016/j.neuron.2004.09.012

Marom, S., & Shahaf, G. (2002). Development, learning and memory in large random networks of cortical neurons: Lessons beyond anatomy. In *Quarterly Reviews of Biophysics* (Vol. 35, Issue 1). https://doi.org/10.1017/S0033583501003742

Mayer, M. L. (2005). Glutamate receptor ion channels. In *Current Opinion in Neurobiology* (Vol. 15, Issue 3 SPEC. ISS.). https://doi.org/10.1016/j.conb.2005.05.004

Mayorquin, L. C., Rodriguez, A. v., Sutachan, J. J., & Albarracín, S. L. (2018). Connexin-mediated functional and metabolic coupling between astrocytes and neurons. In *Frontiers in Molecular Neuroscience* (Vol. 11). https://doi.org/10.3389/fnmol.2018.00118

Miller, E. K., & Wilson, M. A. (2008). All My Circuits: Using Multiple Electrodes to Understand Functioning Neural Networks. In *Neuron* (Vol. 60, Issue 3). https://doi.org/10.1016/j.neuron.2008.10.033

Mölle, M., Marshall, L., Fehm, H. L., & Born, J. (2002). EEG theta synchronization conjoined with alpha desynchronization indicate intentional encoding. *European Journal of Neuroscience*, *15*(5). https://doi.org/10.1046/j.1460-9568.2002.01921.x

Mota, J., Yu, N., Caridade, S. G., Luz, G. M., Gomes, M. E., Reis, R. L., Jansen, J. A., Frank Walboomers, X., & Mano, J. F. (2012). Chitosan/bioactive glass nanoparticle composite membranes for periodontal regeneration. *Acta Biomaterialia*, *8*(11). https://doi.org/10.1016/j.actbio.2012.06.040

Nicholson, C., & Syková, E. (1998). Extracellular space structure revealed by diffusion analysis. *Trends in Neurosciences*, *21*(5). https://doi.org/10.1016/S0166-2236(98)01261-2

No, H. K., & Meyers, S. P. (1995). Preparation and characterization of chitin and chitosan- a review. *Journal of Aquatic Food Product Technology*, *4*(2). https://doi.org/10.1300/J030v04n02_03

Novak, U., & Kaye, A. H. (2000). Extracellular matrix and the brain: Components and function. In *Journal of Clinical Neuroscience* (Vol. 7, Issue 4). https://doi.org/10.1054/jocn.1999.0212

Pai, S. a. (2009). Annual Review of Pathology: Mechanisms of Disease, 2009. In *Current Science (00113891)* (Vol. 97, Issue 6).

Pasquale, V., Martinoia, S., & Chiappalone, M. (2010). A self-adapting approach for the detection of bursts and network bursts in neuronal cultures. *Journal of Computational Neuroscience*, *29*(1–2). https://doi.org/10.1007/s10827-009-0175-1

Petroff, O. A. C. (2002). GABA and glutamate in the human brain. In *Neuroscientist* (Vol. 8, Issue 6). https://doi.org/10.1177/1073858402238515

Prasitsilp, M., Jenwithisuk, R., Kongsuwan, K., Damrongchai, N., & Watts, P. (2000). Cellular responses to chitosan in vitro: The importance of deacetylation. *Journal of Materials Science: Materials in Medicine*, *11*(12). https://doi.org/10.1023/A:1008997311364

Prince, E., & Kumacheva, E. (2019). Design and applications of man-made biomimetic fibrillar hydrogels. In *Nature Reviews Materials* (Vol. 4, Issue 2). https://doi.org/10.1038/s41578-018-0077-9

Quartz, S. R., & Sejnowski, T. J. (1997). The neural basis of cognitive development: A constructivist manifesto. In *Behavioral and Brain Sciences* (Vol. 20, Issue 4). https://doi.org/10.1017/S0140525X97001581

Reubinoff, B. E., Itsykson, P., Turetsky, T., Pera, M. F., Reinhartz, E., Itzik, A., & Ben-Hur, T. (2001). Neural progenitors from human embryonic stem cells. *Nature Biotechnology*, *19*(12). https://doi.org/10.1038/nbt1201-1134

Rodríguez-Vázquez, M., Vega-Ruiz, B., Ramos-Zúñiga, R., Saldaña-Koppel, D. A., & Quiñones-Olvera, L. F. (2015). Chitosan and Its Potential Use as a Scaffold for Tissue Engineering in Regenerative Medicine. In *BioMed Research International* (Vol. 2015). https://doi.org/10.1155/2015/821279

Roth, F. C., & Draguhn, A. (2012). GABA metabolism and transport: Effects on synaptic efficacy. In *Neural Plasticity* (Vol. 2012). https://doi.org/10.1155/2012/805830

Schneidman, E., Freedman, B., & Segev, I. (1998). Ion Channel Stochasticity May Be Critical in Determining the Reliability and Precision of Spike Timing. *Neural Computation*, *10*(7). https://doi.org/10.1162/089976698300017089

Shepherd, G. M. (2004). The Synaptic Organization of the Brain. In *The Synaptic Organization of the Brain*. https://doi.org/10.1093/acprof:oso/9780195159561.001.1

Steriade, M., Amzica, F., & Nunez, A. (1993). Cholinergic and noradrenergic modulation of the slow (≃0.3 Hz) oscillation in neocortical cells. *Journal of Neurophysiology*, *70*(4). https://doi.org/10.1152/jn.1993.70.4.1385

Tang, X., Zhou, L., Wagner, A. M., Marchetto, M. C. N., Muotri, A. R., Gage, F. H., & Chen, G. (2013). Astroglial cells regulate the developmental timeline of human neurons differentiated from induced pluripotent stem cells. *Stem Cell Research*, *11*(2). https://doi.org/10.1016/j.scr.2013.05.002

Tibbitt, M. W., & Anseth, K. S. (2009). Hydrogels as extracellular matrix mimics for 3D cell culture. In *Biotechnology and Bioengineering* (Vol. 103, Issue 4). https://doi.org/10.1002/bit.22361

Tukker, A. M., de Groot, M. W. G. D. M., Wijnolts, F. M. J., Kasteel, E. E. J., Hondebrink, L., & Westerink, R. H. S. (2016). Research article is the time right for in vitro neurotoxicity testing using human iPSC-derived neurons? *Altex*, *33*(3). https://doi.org/10.14573/altex.1510091

Verkhratsky, A., & Nedergaard, M. (2018). Physiology of astroglia. *Physiological Reviews*, *98*(1). https://doi.org/10.1152/physrev.00042.2016

Victor, R. de S., Santos, A. M. da C., de Sousa, B. V., Neves, G. de A., Santana, L. N. de L., & Menezes, R. R. (2020). A review on Chitosan's uses as biomaterial: Tissue engineering, drug delivery systems and cancer treatment. In *Materials* (Vol. 13, Issue 21). https://doi.org/10.3390/ma13214995

Wagenaar, D. A., Pine, J., & Potter, S. M. (2006). An extremely rich repertoire of bursting patterns during the development of cortical cultures. *BMC Neuroscience*, *7*. https://doi.org/10.1186/1471-2202-7-11

Wagenaar, D., Demarse, T. B., & Potter, S. M. (2005). MeaBench: A toolset for multi-electrode data acquisition and on-line analysis. *2nd International IEEE EMBS Conference on Neural Engineering*, *2005*. https://doi.org/10.1109/CNE.2005.1419673

Whitlock, J. R., Heynen, A. J., Shuler, M. G., & Bear, M. F. (2006). Learning induces long-term potentiation in the hippocampus. *Science*, *313*(5790). https://doi.org/10.1126/science.1128134

Wolbarsht, M. L. (1964). The Basis of Sensation. The Action of the Sense Organs. E. D. Adrian . *The Quarterly Review of Biology*, *39*(4). https://doi.org/10.1086/404399